CANCER

Reprogramming of tumor-associated macrophages by targeting β-catenin/FOSL2/ARID5A signaling: A potential treatment of lung cancer

Poonam Sarode[1], Xiang Zheng[1], Georgia A. Giotopoulou[2], Andreas Weigert[3], Carste Kuenne[1], Stefan Günther[1], Aleksandra Friedrich[1], Stefan Gattenlöhner[4], Thorsten Stiewe[5], Bernhard Brüne[3,6], Friedrich Grimminger[7], Georgios T. Stathopoulos[2], Soni Savai Pullamsetti[1,7], Werner Seeger[1,7,8], Rajkumar Savai[1,6,7,8]*

Tumor-associated macrophages (TAMs) influence lung tumor development by inducing immunosuppression. Transcriptome analysis of TAMs isolated from human lung tumor tissues revealed an up-regulation of the Wnt/β-catenin pathway. These findings were reproduced in a newly developed in vitro "trained" TAM model. Pharmacological and macrophage-specific genetic ablation of β-catenin reprogrammed M2-like TAMs to M1-like TAMs both in vitro and in various in vivo models, which was linked with the suppression of primary and metastatic lung tumor growth. An in-depth analysis of the underlying signaling events revealed that β-catenin–mediated transcriptional activation of FOS-like antigen 2 (FOSL2) and repression of the AT-rich interaction domain 5A (ARID5A) drive gene regulatory switch from M1-like TAMs to M2-like TAMs. Moreover, we found that high expressions of β-catenin and FOSL2 correlated with poor prognosis in patients with lung cancer. In conclusion, β-catenin drives a transcriptional switch in the lung tumor microenvironment, thereby promoting tumor progression and metastasis.

INTRODUCTION

Lung cancer is the primary cause of cancer-related death in the United States of America and Europe. Early-stage lung cancer is treatable with radical interventions, but >70% of patients relapse and expire, mostly because of metastatic progression (*1*). Targeted therapies are beneficial to only 15 to 20% of patients with lung cancer harboring drug-sensitive mutations. In these patients, too, resistance development is a major obstruction to a durable therapeutic response. Recent clinical trials with immune checkpoint blockade therapy [Cytotoxic T-Lymphocyte Associated Protein 4 (CTLA-4) and Programmed cell death 1 (PD-1)] demonstrated an unprecedented durable response in patients with various cancers (*2*, *3*). However, only a subset of patients achieves a durable response to immunotherapy. Thus, further in-depth analysis of the entire spectrum of cells in the tumor microenvironment (TME) contributing to lung carcinogenesis is crucial to identify new targeted therapies.

Extensive immunogenomic analysis of >10,000 samples from The Cancer Genome Atlas (comprising 33 diverse cancer types) showed a more prominent macrophage signature with a T helper cell 1–suppressed response in lung tumors (*4*). The high density of tumor-associated macrophages (TAMs) in lung cancer correlates with poor prognosis and reduced overall patient survival (*5*). Our recent work suggests that cytokines and chemokines, secreted through cross-talk between TAMs and tumor cells, strongly induce a hyperproliferative, antiapoptotic, and metastatic response in lung cancer and lung cancer–associated diseases. This finding offers a potential therapeutic option for treating lung cancer (*6*, *7*). However, TAMs exhibit functional heterogeneity ranging from immune-activated, proinflammatory, and antitumor responses to regulatory, anti-inflammatory, and protumoral activities. Their functional heterogeneity is reflected by phenotypic subsets (i.e., tumor-inhibiting M1-like and tumor-promoting M2-like TAMs). Further, their differentiation from monocytes to macrophages, polarization into different subsets, and interconversion within subsets depend on microenvironmental signals. The mechanisms through which TME induces the phenotypic transition of M1-like TAMs to M2-like TAMs remain unclear (*8*, *9*). Thus, identifying the underlying molecular mechanisms responsible for the phenotypic switch of TAMs is urgently needed to design combination therapies that will treat lung cancer by improving immunosurveillance.

Over the past decade, research investigating Wnt pathway aberrations in lung cancer suggests that Wnt activation occurs at a high frequency in non–small cell lung carcinoma (NSCLC) in humans. Wnt/β-catenin signaling is activated in 50% of human NSCLC cell lines and resected lung cancer samples (*10*). Activated Wnt/β-catenin signaling is clinically associated with the stage, size, and grade of tumors, as well as the prognosis and survival of patients with lung cancer (*11*, *12*). Activation of Wnt/β-catenin signaling in lung cancer is a result of co-occurring genetic, epigenetic, and gene expression alterations in lung cancer cells as well as aberrant expressions of

[1]Max Planck Institute for Heart and Lung Research, Member of the German Center for Lung Research (DZL), Member of the Cardio-Pulmonary Institute (CPI), Bad Nauheim 61231, Germany. [2]Laboratory for Molecular Respiratory Carcinogenesis, Department of Physiology, Faculty of Medicine, University of Patras, Rio, 26504, Greece and Lung Carcinogenesis Laboratory, Comprehensive Pneumology Center (CPC) and Institute for Lung Biology and Disease (iLBD), University Hospital, Ludwig-Maximilians University and Helmholtz Center Munich, Member of the German Center for Lung Research (DZL), Munich 81377, Germany. [3]Institute of Biochemistry I, Faculty of Medicine, Goethe University Frankfurt, Frankfurt 60323, Germany. [4]Department of Pathology, Member of the DZL, Justus Liebig University, Giessen 35390, Germany. [5]Institute of Molecular Oncology, Philipps-University Marburg, Member of the DZL, Marburg 35043, Germany. [6]Frankfurt Cancer Institute (FCI), Goethe University, 60596 Frankfurt am Main, Germany. [7]Department of Internal Medicine, Member of the DZL, Member of CPI, Justus Liebig University, 35392 Giessen, Germany. [8]Institute for Lung Health (ILH), Justus Liebig University, 35392 Giessen, Germany.
*Corresponding author. Email: rajkumar.savai@mpi-bn.mpg.de

molecules related to Wnt signaling activity (*13*). Wnt/β-catenin signaling plays a cardinal role in maintaining populations of therapy-resistant cancer stem cells. Therefore, it possibly plays an important role in drug resistance and disease recurrence (*14*). In addition, activating Wnt/β-catenin signaling in tumor cells modulates the recruitment of immune cells, particularly macrophages and T cells in TME (*15*, *16*).

Recent cancer studies (e.g., on breast cancer, colorectal cancer, cholangiocarcinoma, ovarian cancer, and metastatic melanoma) examined the molecular signature of activated Wnt/β-catenin signaling not only in tumor cells but also in tumor-infiltrating $FoxP3^+$ T cells, dendritic cells (DCs), and TAMs, suggesting a bidirectional role of the Wnt/β-catenin pathway in the cross-talk between tumor cells and immune cells (*17*, *18*). However, the role of TAM-specific Wnt/β-catenin signaling in immune evasion in lung cancer has not been systematically investigated. This is also true for the transcriptional landscape mediated by β-catenin along with transcriptional cofactor T cell factor/lymphoid enhancer-binding factor (TCF/LEF; hereafter referred to as TCF) in TAMs including context-dependent activation and repression of various target genes (*19*).

In this study, we present evidence that macrophage-specific β-catenin–mediated Wnt signaling is centrally involved in the phenotypic transition of M1-like TAMs to M2-like TAMs in lung TME. Targeting β-catenin–mediated transcriptional activation of FOS-like antigen 2 (FOSL2) and repression of the AT-rich interaction domain 5A (ARID5A) in M2-like TAMs, as well as partial macrophage gene regulation via tumor necrosis factor (TNF) and CCR2, were found to suppress lung tumor progression/metastasis in three preclinical lung cancer models (xenograft, carcinogen-induced, and metastatic lung tumors), in in vitro trained TAMs and in ex vivo cultured TAMs isolated from mouse and human lung tumors. Moreover, upon analysis of the transcriptomic data of patients with lung cancer, high expressions of β-catenin and FOSL2 and low expression of ARID5A were found to be correlated with poor prognosis. Thus, targeting β-catenin–dependent gene regulation in M2-like TAMs may offer a new treatment strategy in lung cancer.

RESULTS

Wnt/β-catenin signaling is up-regulated in lung TAMs

We developed a flow cytometry sorting protocol based on 8-fluorochrome cell staining to precisely delineate the molecular signature of TAMs isolated from patients with lung cancer and of nontumor macrophages (NMs) isolated from matched control tissues (fig. S1A). RNA sequencing (RNA-seq) of macrophages sorted using fluorescence-activated cell sorting (FACS) revealed different gene expression between TAMs and NMs (Fig. 1A). PANTHER pathway analysis identified the Wnt signaling pathway as one of the pathways most enriched for genes up-regulated in TAMs (Fig. 1B). In accordance, protein expression analysis of Wnt signaling [CTNNB1/β-catenin and tankyrase (TNKS1/2)] and its target genes (CCND1, MYC, and MET) in TAMs and NMs confirmed Wnt/β-catenin signaling activation in TAMs (Fig. 1C). Furthermore, coimmunostaining of β-catenin and a macrophage marker (CD68) in a microarray of human lung tissues revealed that β-catenin was expressed in tumor cells, but it was also highly expressed in TAMs (Fig. 1D). Collectively, these results indicate that Wnt/β-catenin signaling is substantially up-regulated in TAMs in patients with lung cancer.

Wnt/β-catenin signaling significantly activated in in vitro trained M2-like TAMs

Evidence suggests that spatial proximity between tumor cells and TAMs leads to a phenotypic transition of TAMs (*20*, *21*). Accordingly, we developed an in vitro model that mimics this phenotypic alteration of macrophages upon coculture with tumor cells (Fig. 1E). First, we directly cocultured undifferentiated macrophages (M0) with A549 tumor cells for 5 days. However, the cocultured tumor cells underwent apoptosis for 5 days, with the maximum apoptosis observed on day 3 (fig. S1B, black line). Therefore, we decided to remove apoptotic tumor cells daily and replaced them with new tumor cells and cocultured for the subsequent 5 days. The replacement on days 3 to 5 significantly reduced the apoptosis of tumor cells compared with that on days 1 and 2 (fig. S1B, red line). On the other hand, cocultured macrophages showed 80 to 90% cell viability at all time points during the coculturing period (fig. S1C). Further, the mRNA expression profiles of M1 (*TNF*, *IL1B*, and *IL8*) and M2 (*IL10*, *CD163*, and *ALOX15*) macrophage markers in in vitro TAM coculture model highlighted two major observations. First, without the addition of tumor cells, the cocultured macrophages improved the M1 polarization profile until day 3 and later declined it. In contrast, the M2 polarization profile showed a constant increase from days 3 to 5 (fig. S1, D and E, black lines). Second, with the addition of new tumor cells on day 3, the M1 profile transited toward the M2 profile when compared to replacement at day 1 or 2 (fig. S1, D and E, red lines). Therefore, macrophages from 3-day coculture (without cell replacement) were termed as M1-like TAMs and those from 5-day coculture (with cell replacement on day 3) as M2-like TAMs.

We performed a head-to-head comparison of the in vitro TAM coculture model with classical M1 [lipopolysaccharide (LPS) and interferon γ (IFNγ) stimulated] and M2 [interleukin-4 (IL4) stimulated] models over three variables, i.e., phenotypic marker regulation at both mRNA and protein levels as well as characterized their influence on tumor cell functions. Notably, RNA-seq and quantitative reverse transcription polymerase chain reaction (PCR) for M1 (*TNF*, *IL1B*, *IL8*, *IL6*, *IL12*, and *CCR7*) and M2 (*IL10*, *CD163*, *ALOX15*, *MRC1*, *IL1R1*, and *TGFB1*) phenotypic markers suggested the up-regulation of M1 macrophage markers in both classical M1 and M1-like TAMs. Similarly, up-regulation of M2 macrophage markers was observed in classical M2 and M2-like TAMs (Fig. 1F and fig. S1, F and G), suggesting a similar regulation of the phenotypic markers in both classical and in vitro TAM coculture model. Both FACS analysis of cell surface phenotypic markers (CD80 and CD163) (fig. S1H) and Western blotting of both M1 and M2 phenotypic markers (IL12, IL10, CD163, and ALOX15) (fig. S1I), as well as secretome analysis of phenotypic markers (TNF and IL10) (Fig. 1G), confirmed the similarities in the regulation of phenotypic markers between classical M1/M2 and in vitro trained M1-like/M2-like TAMs. Further, the conditioned medium (CM) from M0, classical M1, classical M2, M1-like TAMs, and M2-like TAMs demonstrated that compared with CM from M0, that from classical M1 and M1-like TAMs induces apoptosis of A549 cells (Fig. 1H). In contrast, CM from classical M2 and M2-like TAMs induced the proliferation and migration of A549 cells (Fig. 1, I and J). Notably, CM from human primary lung cancer cells and other lung tumor cells such as A427 and H1650, which were cocultured with macrophages, also displayed a significant increase in the proliferation and migration of tumor cells by CM of M2-like TAMs compared with their M1 counterparts (fig. S2, A to C). Although some similarities were observed between

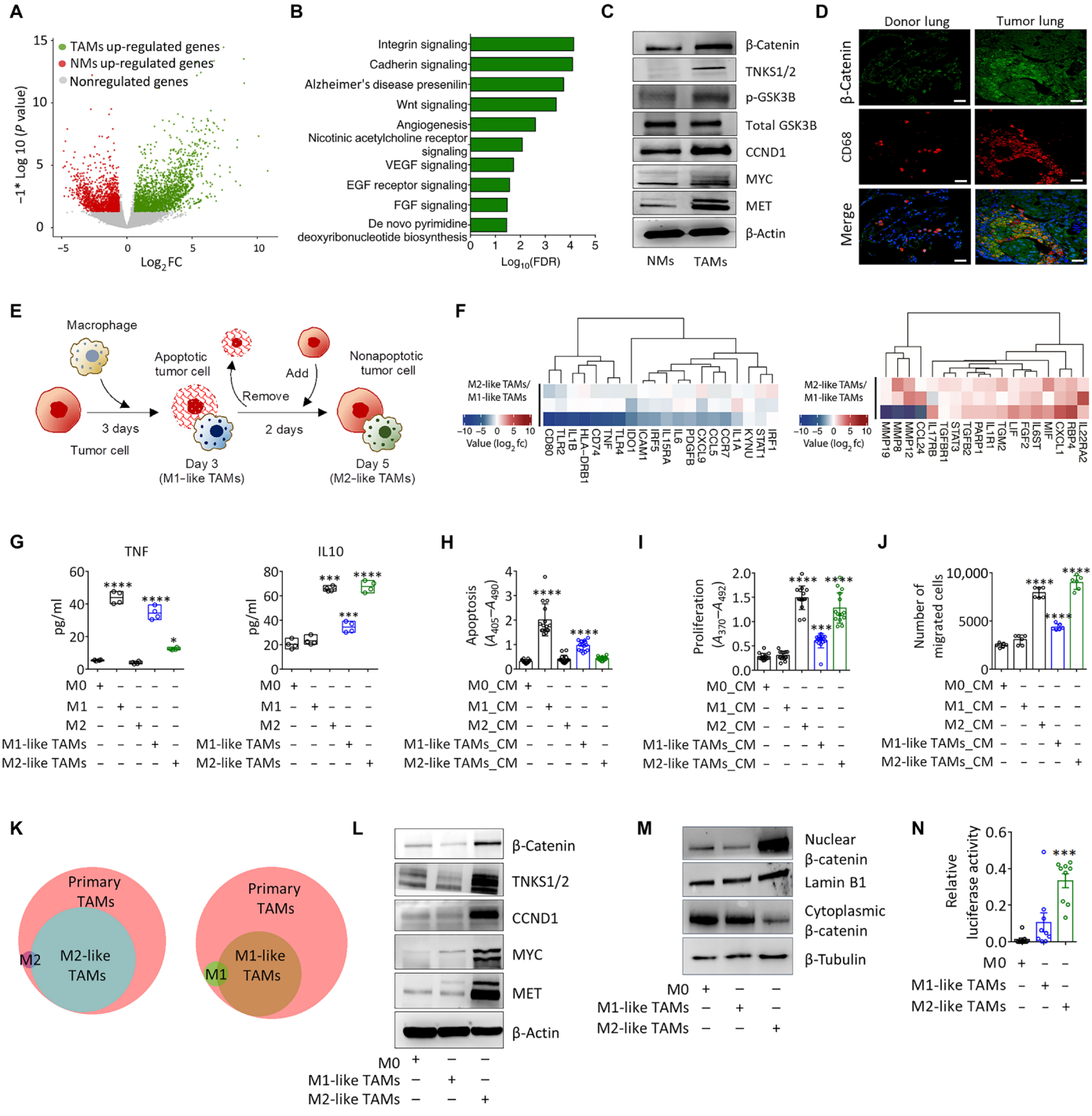

Fig. 1. Activation of Wnt/β-catenin signaling in primary and in vitro trained M2-like TAMs. (**A**) Volcano plot showing differentially expressed genes (DEGs) in TAMs versus NMs, $n = 5$. FC, fold change. (**B**) Top 10 panther pathways in TAMs–up-regulated DEGs. VEGF, vascular endothelial growth factor; EGF, epidermal growth factor; FGF, fibroblast growth factor. (**C**) Western blot of Wnt/β-catenin signaling genes in primary TAMs and NMs. (**D**) Representative immunofluorescence images of donors ($n = 2$) and lung cancer tissues ($n = 70$) in lung tissue microarray. Scale bars, 50 μM. (**E**) Scheme depicting generation of in vitro trained TAMs. (**F**) Heatmaps display M1 and M2 macrophage markers' expression in M1-like and M2-like TAMs, $n = 3$. (**G**) Enzyme-linked immunosorbent assay (ELISA)–based quantification of TNF and IL10 in M0, M1, M2, and A549-trained M1-like and M2-like TAMs, $n = 4$, $^{*}P < 0.05$, $^{***}P < 0.001$, $^{****}P < 0.0001$ versus M0. (**H**) Apoptosis, (**I**) proliferation, and (**J**) migration of A549 in the presence of CM from M0, M1, M2, and A549-trained M1-like and M2-like TAMs, $n = 9$, $^{***}P < 0.001$, $^{****}P < 0.0001$ versus M0-CM. (**K**) Venn diagram showing overlap of up-regulated DEGs by combined RNA-seq analysis of primary TAMs, classical macrophages, and in vitro TAMs. (**L**) Western blot of Wnt/β-catenin signaling genes in M0 and A549-trained M1-like and M2-like TAMs. (**M**) Western blot of nuclear, cytoplasmic β-catenin, Lamin B1, and β-tubulin. (**N**) Relative TCF/LEF luciferase activity in M0 and A549-trained M1-like and M2-like TAMs, $n = 9$, $^{***}P < 0.001$ versus M0.

classical macrophages and in vitro trained TAMs, to see how relevant the classical M1/M2 and the in vitro trained TAMs (M1-like TAMs/M2-like TAMs) to primary human TAMs, we performed the RNA-seq from all the above conditions and checked how many genes are similarly up-regulated in each condition as to primary human TAMs. We have observed that M1-like TAMs/M2-like TAMs mimic the complexity of human TAMs, at least at the level of gene regulation as compared to classical M1/M2 (Fig. 1K). Collectively, these results confirmed a new in vitro TAMs model that depicts the phenotypic and functional transition of M1-like TAMs to M2-like TAMs, leading to increased proliferation, migration, and decreased apoptosis of tumor cells.

Notably, similar to primary TAMs, PANTHER pathway analysis identified the Wnt signaling pathway as one of the significantly enriched pathways in M2-like TAMs (fig. S2D). The most common stimulatory modifications of Wnt/β-catenin signaling [Wnt family members (WNTs), Dishevelleds (DVLs), Lymphoid enhancer-binding factor (LEF1), etc.] and its target genes (Myc, cyclin D1, IDs, etc.) (fig. S2E) were up-regulated in M2-like TAMs compared with those in M1-like TAMs. In addition, mRNA expression profiling of Wnt molecules confirmed the up-regulation of WNT ligands (*WNT5A*, *WNT7B*, and *WNT11*), frizzled receptors (*FZD4*, *FZD5*, *FZD6*, *FZD8*, and *FZD9*), disheveled (*DVL2* and *DVL3*), and *TNK1/2* exclusively in M2-like TAMs (fig. S2F). Western blot analysis of Wnt/β-catenin signaling (β-catenin and TNKS1/2) and its target genes (CCND1, MYC, and MET) (Fig. 1L) confirmed the up-regulation of the Wnt/β-catenin pathway in M2-like TAMs compared with that in M1-like TAMs. Moreover, TAMs trained through coculture with A427, H1650, and primary lung tumor cells showed up-regulation of the Wnt/β-catenin pathway in M2-like TAMs compared with that in M1-like TAMs (fig. S2G). The increased expression of nuclear β-catenin while decreased expression of cytoplasmic β-catenin (Fig. 1M) and increased TCF/LEF activity (Fig. 1N) in M2-like TAMs compared with M0 and M1-like TAMs further confirmed the activation of the Wnt/β-catenin pathway in M2-like TAMs. Collectively, these results show the significant activation of Wnt/β-catenin signaling in in vitro trained M2-like TAMs, indicating that it may be the underlying molecular mechanism responsible for the transition of M1-like TAMs to M2-like TAMs.

Inhibition of β-catenin leads to a phenotypical and functional transition of tumor-promoting M2-like TAMs to tumor-inhibiting M1-like TAMs

M2-like TAMs were transfected with β-catenin short hairpin RNA (shRNA; sh_β-catenin) for 24 hours to test whether Wnt/β-catenin signaling is a crucial molecular mechanism responsible for the transition of M1-like TAMs to M2-like TAMs. Decreased protein expression of Wnt/β-catenin signaling (β-catenin and TNKS1/2) and its target genes (CCND1, MYC, and MET) demonstrated the down-regulation of nuclear β-catenin activity in M2-like TAMs transfected with sh_β-catenin (Fig. 2A). Notably, the mRNA expression of M1 macrophage markers was up-regulated, whereas that of M2 macrophage markers was down-regulated in M2-like TAMs transfected with sh_β-catenin, demonstrating the phenotypic transition of M2-like TAMs to M1-like TAMs (Fig. 2B and fig. S3A). In addition, the treatment of A549 cells with CM from M2-like TAMs transfected with sh_β-catenin showed increased apoptosis (Fig. 2C) and reduced proliferation (Fig. 2D) and migration (Fig. 2E), further confirming the functional transition of M2-like TAMs to M1-like TAMs. Moreover, small interfering RNA (siRNA)–mediated knockdown of β-catenin in ex vivo TAMs isolated from human lung tumors for 24 hours down-regulated the mRNA expression of *CCND1* (Fig. 2F). Similar to M2-like TAMs, ex vivo TAMs transfected with si_β-catenin also showed increased expression of M1 and decreased expression of M2 macrophage markers (Fig. 2G and fig. S3B). Further, their CM decreased the survival and proliferation of primary tumor cells (Fig. 2H).

Similar to genetic ablation of β-catenin, pharmacological blockade using a cell-permeable small-molecule inhibitor (XAV939) in ex vivo TAMs isolated from human/mouse lung tumors consistently resulted in the down-regulation of *CCND1* and M2 macrophage markers and the up-regulation of M1 macrophage markers (Fig. 2, I and J, and fig. S3, C to E). Furthermore, the treatment of human primary lung tumor cells and mouse lung cancer cell lines with CM from XAV939-treated human ex vivo TAMs and mouse ex vivo TAMs decreased their survival and proliferation (Fig. 2K and fig. S3F). In addition, CM from XAV939-treated M2-like TAMs (trained in vitro by coculturing with A427 and H1650) decreased the survival and proliferation of A427 and H1650 cells compared with CM from untreated M2-like TAMs (fig. S3, G and H). As a control, M1-like TAMs were treated with XAV939 for 24 hours, and then, mRNA expression profiling of macrophage markers and functional studies on A549 cells were conducted. Nuclear β-catenin activity (TCF/LEF activity–based) and expression of M2 macrophage markers decreased, whereas those of M1-macrophage markers further increased in XAV939-treated M1-like TAMs (fig. S3, I to K). CM from XAV939-treated M1-like TAMs reduced the proliferation and survival of A549 cells (fig. S3L). Collectively, these results strongly demonstrate that the genetic and pharmacological ablation of β-catenin shifts tumor-promoting M2-like TAMs to tumor-inhibiting M1-like TAMs.

A549 cells were treated with various concentrations of XAV939 (0, 1, 2, 4, 8, 16, 32, 64, and 128 μM) or CM from XAV939-treated (0, 1, 2, 4, and 8 μM) M2-like TAMs to compare the effects of direct versus indirect (via TAM manipulation) β-catenin blockade on the tumorigenicity of A549 cells. To achieve 50 to 60% reduction in the proliferation and survival of tumor cells, we needed a higher concentration of XAV939 (32 to 64 μM) (fig. S4A), whereas to reveal the antitumor response in M2-like TAMs, lower concentrations of XAV939 (4 to 8 μM) were required to obtain similar responses (fig. S4B). These results demonstrated that reactivating the antitumor immunity of TME by inhibiting the TAM-specific Wnt/β-catenin pathway might require significantly lower amounts of the drug than that by directly targeting cancer cells using this inhibitor approach. In addition, to study whether targeting the Wnt/β-catenin pathway in tumor cells is sufficient to prevent M2 polarization of TAMs, we assessed the expression of the polarization markers from macrophages that were subjected to CM from A549 cells transfected with si_β-catenin (fig. S4C). We did not observe any changes in the macrophage polarization status after β-catenin inhibition in tumor cells (fig. S4, D and E).

Pharmacological ablation of β-catenin suppresses primary and metastatic tumor growth by reprogramming TAMs into tumor-inhibiting M1-like TAMs

To determine the functional role of β-catenin inhibition in vivo, we used XAV939 (25 mg/kg, intraperitoneally) in three different tumor models: (i) subcutaneous tumors, (ii) carcinogen-induced lung tumors, and (iii) metastatic lung tumors. Treatment with XAV939 significantly reduced the growth of primary (subcutaneous and carcinogen-induced) and metastatic (macroscopic and microscopic)

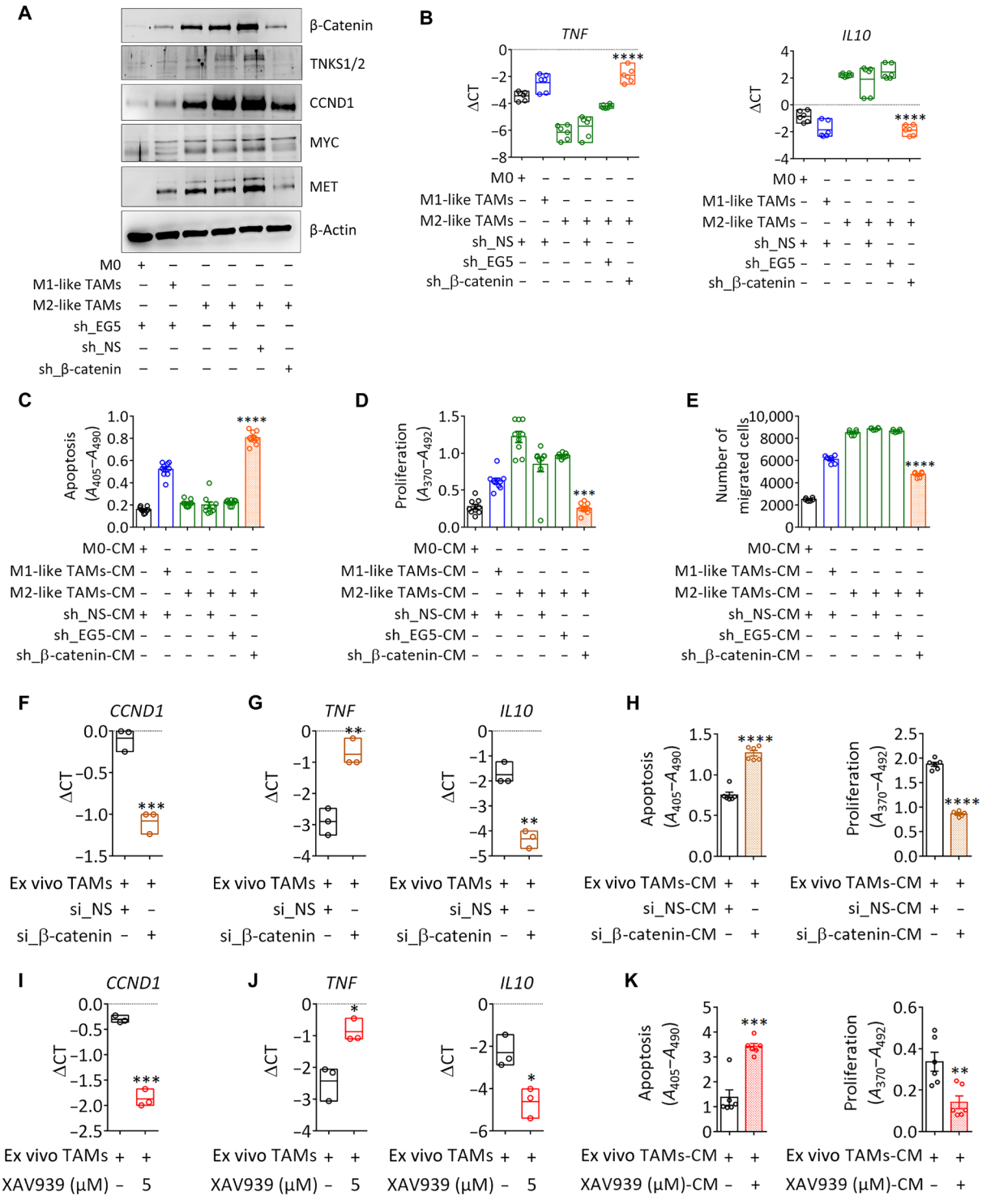

Fig. 2. Genetic and pharmacological ablation of β-catenin in vitro trained and primary TAMs switches M2-like TAMs to M1-like TAMs. (**A**) Western blot of Wnt/β-catenin signaling genes. (**B**) mRNA expression of *TNF* and *IL10* in M0, M1-like, and M2-like TAMs transfected with sh_NS, sh_EG5, and sh_β-catenin for 24 hours, $n = 6$. (**C**) Apoptosis, (**D**) proliferation, and (**E**) migration of A549 in the presence of CM from M0, M1-like, and M2-like TAMs transfected with sh_NS, sh_EG5, and sh_β-catenin for 24 hours; $n = 9$, $^{***}P < 0.001$, $^{****}P < 0.0001$ versus sh_NS or sh_NS-CM. mRNA expression of (**F**) *CCND1*, (**G**) *TNF*, and *IL10* in ex vivo TAMs transfected with si_NS (nonsilencing control siRNA) and si_β-catenin for 24 hours, $n = 6$. (**H**) Apoptosis and proliferation of primary tumor cells in the presence of CM from ex vivo TAMs transfected with si_NS and si_β-catenin for 24 hours, $n = 6$, $^{**}P < 0.01$, $^{***}P < 0.001$, $^{****}P < 0.0001$ versus si_NS or si_NS-CM. mRNA expression of (**I**) *CCND1*, (**J**) *TNF*, and *IL10* in ex vivo TAMs treated with XAV939 for 24 hours, $n = 6$. (**K**) Apoptosis and proliferation of primary tumor cells in the presence of CM from ex vivo TAMs treated with XAV939 for 24 hours, $n = 6$, $^{*}P < 0.05$, $^{**}P < 0.01$, $^{***}P < 0.001$ versus ex vivo TAM or ex vivo TAM-CM.

lung tumors in vivo (Fig. 3, A to C, and fig. S5, A to C). To delineate the TAMs' molecular signature of the control [dimethyl sulfoxide (DMSO)] versus XAV939-treated groups, primary TAMs were isolated using F4/80 antibody-linked magnetic beads, followed by mRNA expression profiling. The reduced mRNA expression of *Ccnd1* in TAMs isolated from XAV939-treated animals confirmed the down-regulation of nuclear β-catenin activity in these in vivo studies (fig. S5, D to F). Notably, TAMs isolated from the XAV939 group showed increased expression of M1 macrophage markers (*Tnf*, *Nos2*, and *Il1b*) and decreased expression of M2 macrophage markers (*Il10*, *Arg1*, and *Chit1*) (Fig. 3, D to F, and fig. S5, G to L). Moreover, treatment with XAV939 significantly reduced the number of $CD206^+$ M2-like TAMs in TME (Fig. 3, G to I). Collectively, these results indicate that inhibiting β-catenin restricts tumor growth in vivo. β-Catenin down-regulation in TAMs induces their phenotypical transition into tumor-inhibiting M1-like TAMs in TME in different lung cancer models.

Macrophage-specific genetic ablation of β-catenin reduces lung tumor development by inducing M1-like TAM–directed antitumor immunity in TME

We hypothesized that inactivating β-catenin in TAMs switches the phenotype to that of M1-like TAMs, thereby inducing functional antitumor immunity in lung TME. To test this hypothesis, transgenic mice with macrophage-specific β-catenin depletion ($Catnb^{f/f}Lysm^{Cre}$) were developed. Bone marrow–derived M0 macrophages from $Catnb^{f/f}Lysm^{Cre}$ mice have 50 to 60% decreased levels of β-catenin compared with $Lysm^{Cre}$ mice (fig. S6A). We subsequently used two different approaches to induce lung tumors in these transgenic mice. In the first approach, carcinogen-induced models, $Lysm^{Cre}$, $Catnb^{f/f}$, and $Catnb^{f/f}Lysm^{Cre}$ mice, were intraperitoneally treated with urethane for 6 months. In the second approach, bone marrow cells isolated from $Lysm^{Cre}$, $Catnb^{f/f}$, and $Catnb^{f/f}Lysm^{Cre}$ mice were transplanted into these lethally irradiated wild-type (WT) mice; then, Lewis lung carcinoma 1 (LLC1) cells were intratracheally injected into mice. In both models, mice with β-catenin–deficient macrophages ($Catnb^{f/f}Lysm^{Cre}$) showed a significant reduction in macroscopic and microscopic lung tumor burden compared with WT mice ($Lysm^{Cre}$ and $Catnb^{f/f}$) (Fig. 3, J and K, and fig. S6, B and C). Reduced *Ccnd1* mRNA expression confirmed the down-regulation of nuclear β-catenin activity in β-catenin–deficient TAMs (fig. S6, D and E). Notably, $TAM\_Catnb^{f/f}Lysm^{Cre}$ showed increased expression of M1 macrophage markers and decreased expression of M2 macrophage markers (Fig. 3, L and M, and fig. S6, F to I). The tumors in mice bearing β-catenin–deficient macrophages also showed a significant reduction of CD206-positive M2-like TAM infiltration (fig. S6, J and K). Collectively, these results indicate that inhibiting macrophage-specific β-catenin significantly reduced lung tumorigenesis by inducing an antitumor response in M2-like TAMs in TME.

Reprogramming of M2-like TAMs to M1-like TAMs upon β-catenin inhibition is partially dependent on CCR2/β-catenin axis and TNFα

Previously, we demonstrated that macrophage-tumor cells cross-talk via CCR2/CX3CR1 signaling play a key role in lung cancer progression (*6*); we explored the cross-talk between CCR2/CX3CR1 and β-catenin pathways in driving the macrophage gene regulation. The mRNA and protein expression of β-catenin, CCND1, and CCR2 decreased upon genetic ablation of β-catenin ($M0\_Catnb^{f/f}Lysm^{Cre}$), CCR2 ($M0\_Catnb^{f/f}Lysm^{Cre}$) in bone marrow–derived mouse macrophages, and upon pharmacological inhibition of CCR2 (via RS 504393, 5 μM) in human in vitro M2-like TAMs (Fig. 4, A to C, and fig. S7A), confirming a positive feedback loop in β-catenin and CCR2, as demonstrated by Ou *et al.* (*22*). Unlike β-catenin depletion, CCR2 depletion resulted in the regulation of only a few M1 (*TNF* and *Nos2*) and M2 (*IL10* and *CD163*) macrophage markers (Fig. 4, D and E, and fig. S7, B and C). These results indicate that transcriptional regulation of macrophage genes is not entirely dependent on CCR2-mediated β-catenin activation.

Emerging evidence demonstrates that TNF suppresses the gene expression of M2 macrophage's genes (*23*–*25*). In vitro TAMs model showed a decline in expression of TNF matches with increased expression of M2 markers (fig. S1, D and E), and inhibition of β-catenin in M2-like macrophages consistently showed an increase in expression of TNF. Thus, to determine whether the switching of macrophage phenotype is entirely dependent on β-catenin–modulated TNF, we performed siRNA-mediated down-regulation of TNF in β-catenin_KO macrophages ($M0\_Catnb^{f/f}Lysm^{Cre}$ + si_TNF) and M2-like TAMs transfected with si_β-catenin (M2-like TAMs_ si_β-catenin + si_TNF) (Fig. 4, F and G). The down-regulation of TNF increased the expressions of certain M2 macrophage markers (*IL0* and *MRC1*) (Fig. 4, H and J), whereas expression of other M2 macrophage markers (*ALOX15*, *CD163*, *Arg1*, and *Chit1*) remained unchanged (Fig. 4, I and K). These results are consistent with those reported by Kratochvill *et al.* (*23*) that TNF suppresses expression of M2 macrophage genes in a gene-specific way. In conclusion, these results also suggest that β-catenin via TNF regulates certain M2 macrophage genes, and an additional β-catenin–mediated mechanism may be responsible for the activation of other M2 macrophage genes and suppression of M1 macrophage genes in M2-like TAMs.

β-Catenin differentially regulates the transcription of FOSL2 and ARID5A in M2-like TAMs

RNA-seq was performed on M2-like TAMs transfected with sh_β-catenin to understand the molecular mechanism underlying the phenotypic transition of M2-like TAMs to M1-like TAMs following the inhibition of β-catenin. As shown in the Fig. 5A heatmap, most M1 macrophage markers were up-regulated, whereas M2 macrophage markers were down-regulated in M2-like TAMs transfected with sh_β-catenin. Notably, RNA-seq data revealed the differential expression of transcription factors (TFs) between M2-like TAMs transfected with sh_β-catenin and those transfected with sh_control (Fig. 5B). In silico analysis of the TCF-binding motif ($^{A}/_{A}{}_{T}/_{T}$CAAAG) in these TFs predicted that β-catenin could bind to the promoter regions of FOSL2, recombination signal binding protein for immunoglobulin kappa J (RBPJ), PR/SET domain 1 (PRDM1), Kruppel like factor 9 (KLF9), Transcription factor EC (TFEC), MAX dimerization protein (MGA), Forkhead box J3 (FOXJ3), Kruppel like factor 12 (KLF12), and Cyclic adenosine monophosphate (cAMP) response element–binding protein 5 (down-regulated TFs in M2-like TAMs transfected with sh_β-catenin) as well as Transcription factor EB (TFEB), Upstream transcription factor 1 (UTF1), RELB Proto-oncogene, NF-KB subunit (RELB), and Basic leucine zipper ATF-like transcription factor (BATF) (up-regulated TFs in M2-like TAMs transfected with sh_β-catenin). TF-binding site motif enrichment scanning (TFBS) was performed on the promoter sequences of M1 and M2 macrophage genes to reveal the role of these TFs in the macrophage transcriptional program. Notably, compared with other TFs, FOSL2 and ARID5A exhibited the most significant enrichment of TFBS in the promoter regions of M2 and M1 macrophage genes, respectively (Fig. 5C). In addition, mRNA expression profiling

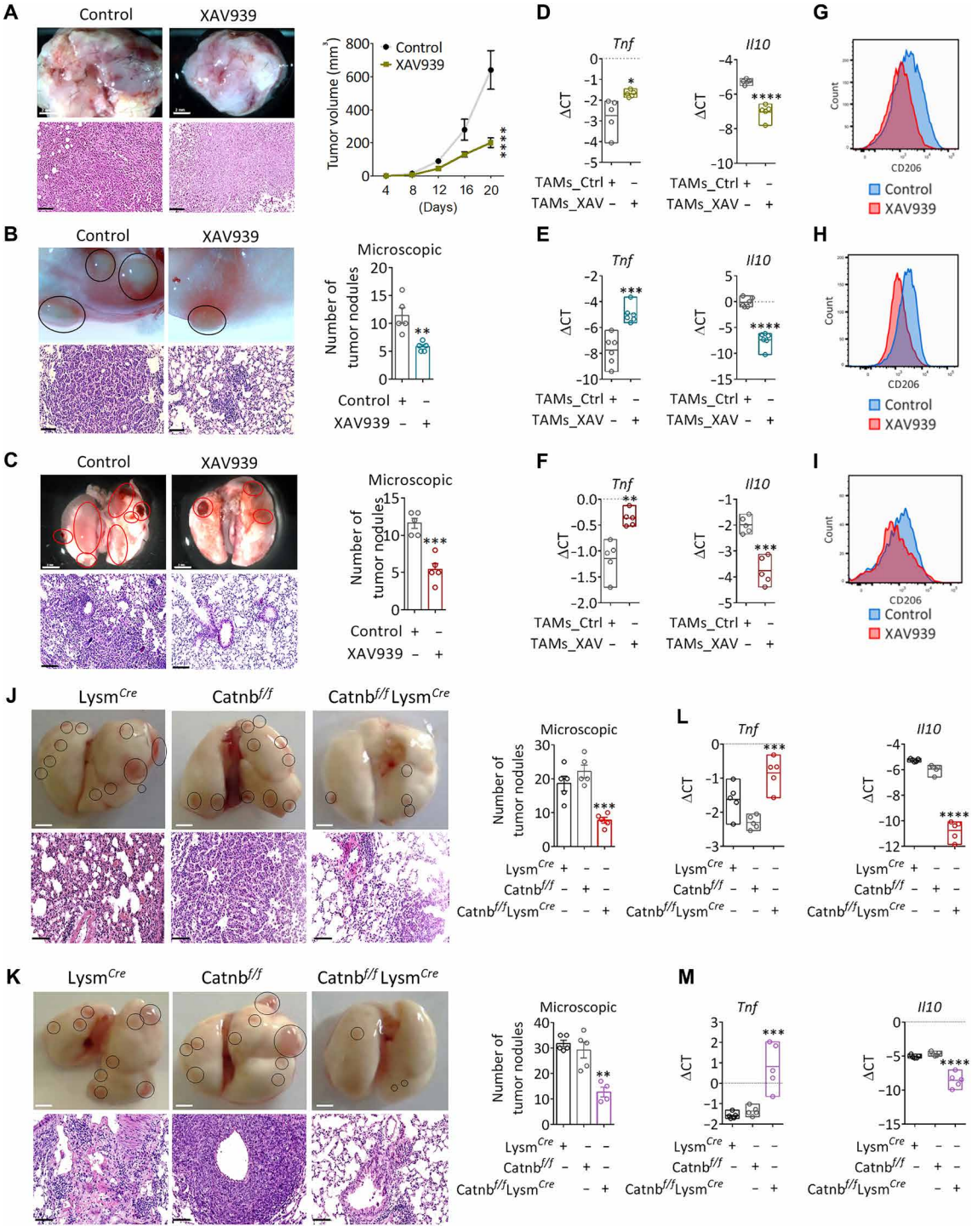

Fig. 3. Pharmacological and macrophage-specific genetic ablation of β-catenin reduces development of lung tumors by reprogramming M2-like to M1-like TAMs in TME. Representative pictures and images of hematoxylin-eosin-stained sections of tumor and quantification of (**A**) subcutaneous tumor and microscopic lung tumor nodules in (**B**) metastasis (**C**) carcinogen-induced lung tumor models. Scale bars, 20 μM, $n = 5$, $^{**}P < 0.01$, $^{***}P < 0.001$, $^{****}P < 0.0001$ versus control. (**D** to **F**) mRNA expression of *Tnf* and *Il10* in TAMs from mice tumor tissue treated with control (DMSO; TAM_Ctrl) and XAV939 (TAM_XAV) in (D) subcutaneous tumor, (E) metastatic, and (F) carcinogen-induced lung tumor models, $n = 5$, $^{*}P < 0.05$, $^{**}P < 0.01$, $^{***}P < 0.001$ versus TAM_Ctrl. (**G** to **I**) FACS histograms indicate mean fluorescence intensity of $CD206^{+}$ macrophages in control and XAV939-treated tumor tissue from (G) subcutaneous tumor, (H) metastatic, and (I) carcinogen-induced lung tumor models. Representative pictures and images of hematoxylin and eosin–stained sections of lungs and quantification of microscopic lung tumor nodules in (**J**) carcinogen-induced and (**K**) bone marrow transplantation models in $Lysm^{Cre}$, $Catnb^{f/f}$, and $Catnb^{f/f}Lysm^{Cre}$ mice. Scale bars, 20 μm, $n = 5$, $^{**}P < 0.01$, $^{***}P < 0.001$ versus $Catnb^{f/f}$. (**L** and **M**) mRNA expression of *Tnf* and *Il10* in TAMs sorted from macrophage-specific β-catenin–deficient tumors (TAM_$Catnb^{f/f}Lysm^{Cre}$) and WT tumors (TAM_$Lysm^{Cre}$ and TAM_$Catnb^{f/f}$) in (L) carcinogen-induced and (M) bone marrow transplant (BMT) lung tumor models, $n = 5$, $^{***}P < 0.001$, $^{****}P < 0.0001$ versus $Catnb^{f/f}$.

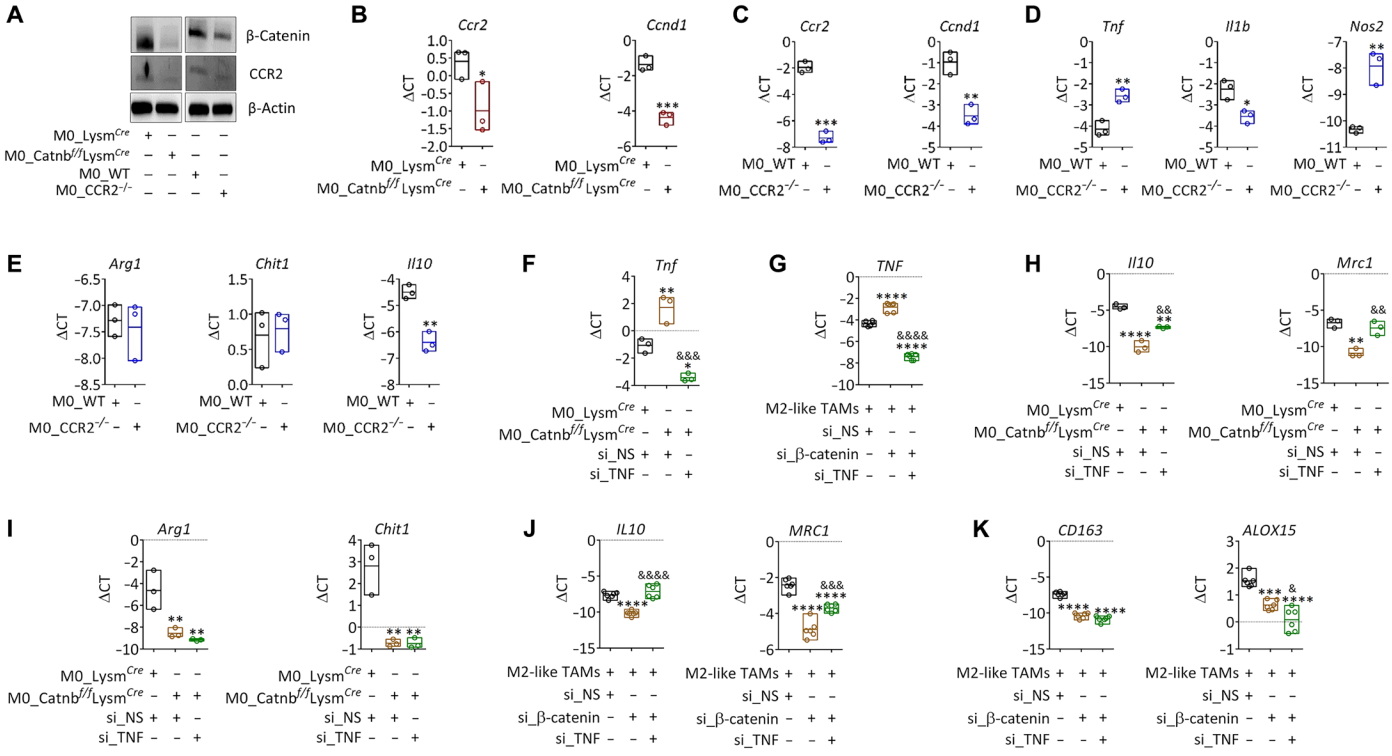

Fig. 4. Reprogramming of M2-like to M1-like TAMs upon β-catenin inhibition is incompletely dependent on CCR2/β-catenin axis and TNFα. (**A**) Western blot of β-catenin and CCR2 in BMDMs from WT, Lysm^{Cre}, Catnb$^{f/f}$Lysm^{Cre}, and CCR2$^{-/-}$ mice. mRNA expressions of *Ccnd1* and *Ccr2* in BMDM from (**B**) Lysm^{Cre}, Catnb$^{f/f}$ Lysm^{Cre}, (**C**) WT, and CCR2$^{-/-}$ mice, $n = 3$, $^{*}P < 0.05$, $^{**}P < 0.01$, $^{***}P < 0.001$ versus M0_Lysm^{Cre} or M0_WT. mRNA expressions of (**D**) *Tnf*, *Nos2*, *Il1b*, (**E**) *Il10*, *Arg1*, and *Chit1* in BMDMs from WT and CCR2$^{-/-}$, $n = 3$, $^{*}P < 0.05$, $^{**}P < 0.01$ versus M0_WT. mRNA expression of (**F**) *Tnf* in M0_Lysm^{Cre} with si_NS and M0_ Catnb$^{f/f}$Lysm^{Cre} with si_NS or si_TNFα for 24 hours, $n = 3$, $^{*}P < 0.05$, $^{**}P < 0.01$ versus M0_Lysm^{Cre}_si_NS, &&&$P < 0.001$ versus M0_Catnb$^{f/f}$Lysm^{Cre}_si_NS. (**G**) *TNF* in M2-like TAMs with si_NS, si_β-catenin and si_β-catenin followed by si_TNFα, $n = 6$, $^{****}P < 0.0001$ versus si_NS, &&&&$P < 0.0001$ versus si_β-catenin. mRNA expression of (**H**) *Il10*, *Mrc1*, (**I**) *Arg1*, and *Chit1* in M0_Lysm^{Cre} with si_NS, M0_ Catnb$^{f/f}$Lysm^{Cre} with si_NS or si_TNFα for 24 hours, $n = 3$, $^{**}P < 0.001$, $^{****}P < 0.0001$ versus M0_Lysm^{Cre}_si_NS, &&$P < 0.01$ versus M0_Catnb$^{f/f}$Lysm^{Cre}_si_NS. (**J**) *IL10*, *MRC1*, (**K**) *CD163*, and *ALOX15* in M2-like TAMs with si_NS, si_β-catenin and si_β-catenin followed by si_TNFα, $n = 6$, $^{****}P < 0.0001$ versus si_NS, &$P < 0.05$, &&&$P < 0.001$, &&&&$P < 0.0001$ versus si_β-catenin.

of these TFs in undifferentiated bone marrow–derived macrophages (BMDMs) (M0) isolated from Lysm^{Cre}, Catnb$^{f/f}$, and Catnb$^{f/f}$Lysm^{Cre} mice showed significant down-regulation of *Fosl2* and up-regulation of *Arid5a* in β-catenin–deficient macrophages (M0_Catnb$^{f/f}$Lysm^{Cre}) compared with other TFs (Fig. 5D and fig. S8A). Corresponding effects were observed for FOSL2 and ARID5A at the protein level (Fig. 5E). β-Catenin–deficient M1-like TAMs, isolated from five different in vivo tumor models (TAMs from Catnb$^{f/f}$Lysm^{Cre} and TAMs from XAV393), also showed the down-regulation of *Fosl2* and up-regulation of *Arid5a* at the mRNA level (Fig. 5, F and G, and fig. S8, B to D). Furthermore, the analysis of mRNA and protein expressions in M1 macrophages, M2 macrophages, M1-like TAMs, and M2-like TAMs confirmed higher expression of FOSL2 in M2 macrophages and M2-like TAMs as well as ARID5A in M1 macrophages and M1-like TAMs (Fig. 5, H and I, and fig. S8, E and F).

To determine whether β-catenin directly binds to the promotor regions of FOSL2 and ARID5A, the promoter occupancy by β-catenin was determined through chromatin immunoprecipitation (ChIP) using a β-catenin antibody in M2 macrophages treated with control (DMSO) and XAV939 (Fig. 5J). Strong enrichment of β-catenin was observed at the promoter regions of FOSL2 and ARID5A and in known β-catenin target genes (IL10, CCND1, and MYC) in M2 macrophages. XAV939 significantly impaired the binding of β-catenin to the promoter regions of the aforementioned target genes (Fig. 5K and fig. S8G). Collectively, these results indicate that β-catenin–induced transcriptional regulation may play a role in M2-like TAM polarization.

β-Catenin–mediated activation of FOSL2 and repression of ARID5A activate tumor-promoting M2-like TAMs in lung cancer

β-Catenin gain of function (OE_β-catenin) and loss of function (si_β-catenin) were performed in M2-like TAMs to explore the β-catenin–mediated transcriptional regulation of FOSL2 and ARID5A. The mRNA and protein expressions of FOSL2 were found to be up-regulated in M2-like TAMs overexpressing β-catenin. In contrast, FOSL2 expression was down-regulated in M2-like TAMs transfected with si_β-catenin. ARID5A showed opposite findings in each of these studies. These findings demonstrated that β-catenin acts as a transcriptional activator and repressor of FOSL2 and ARID5A, respectively (Fig. 6, A and B, and fig. S9, A and B).

Moreover, siRNA-mediated knockdown of FOSL2 was performed in M2-like TAMs to probe further FOSL2's transcriptional role in the polarization of M2-like TAMs (Fig. 6C and fig. S9C). The mRNA expression of various M2 macrophage markers (*MRC1*, *CD163*, *IL1R1*, and *TGFB1*) was significantly down-regulated (Fig. 6D), whereas that of certain M2 (*IL10* and *ALOX15*) and M1 macrophage markers

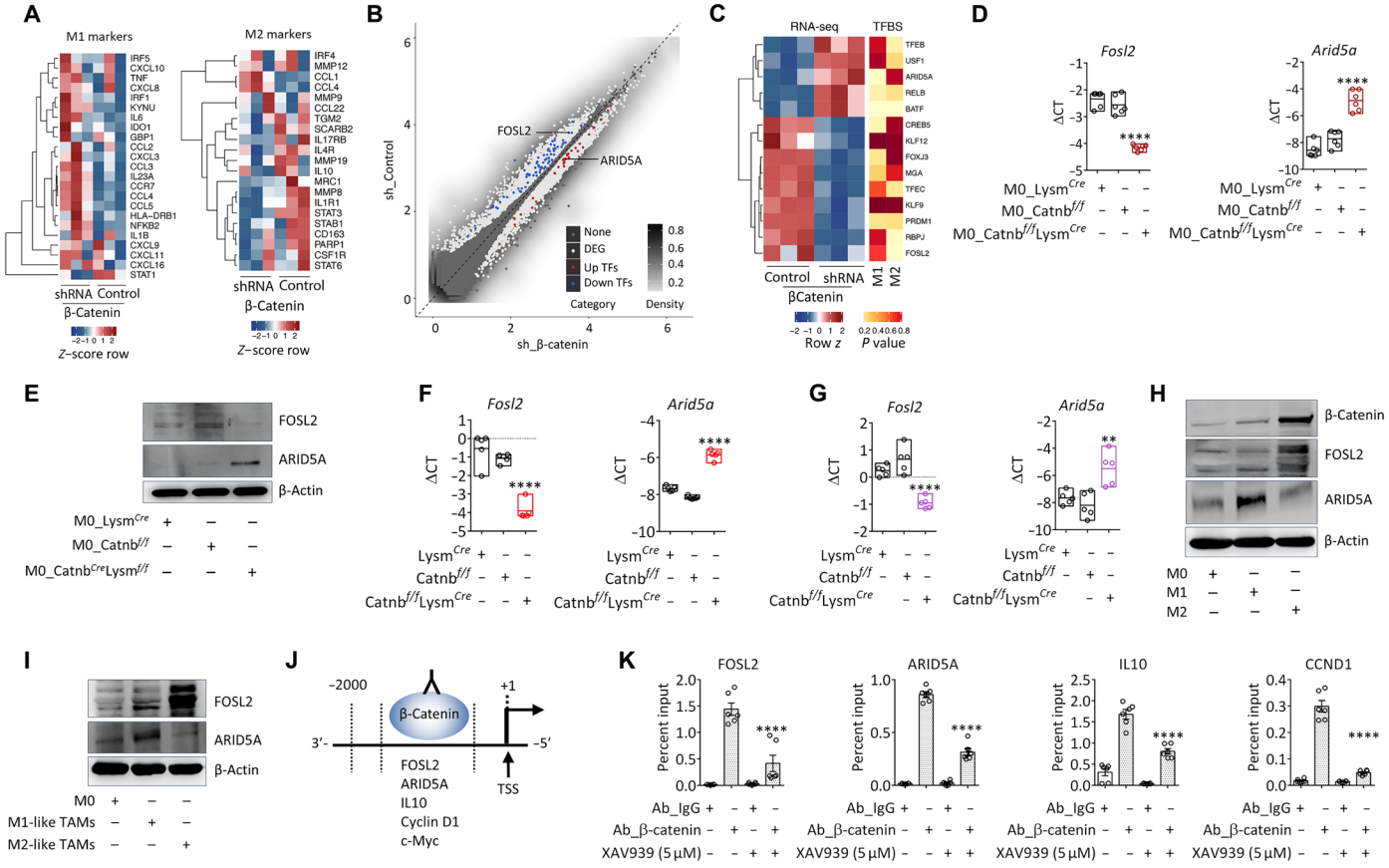

Fig. 5. Dual transcriptional role of β-catenin in the phenotypic transition to M2-like TAMs. (**A**) Heatmaps display M1 and M2 macrophage markers expression in M2-like TAMs transfected with sh_Control and sh_β-catenin, $n = 3$. (**B**) DESeq normalized read count averages of genes were $\log_{10}$ transformed and compared between sh_β-catenin and sh_Control. DEGs (light gray), TFs (annotated by JASPAR; blue and red), and nondifferential genes (dark gray) are depicted as points. (**C**) Left heatmap displays a row-wise *Z* score of RNA-seq. Right heatmap shows Pscan of TF-binding site enrichment *P* value. (**D**) mRNA expression and (**E**) Western blot of FOSL2 and ARID5A in undifferentiated BMDM from Lysm^{Cre}, Catnb$^{f/f}$, and Catnb$^{f/f}$Lysm^{Cre}, $n = 6$, ****$P < 0.0001$ versus Catnb$^{f/f}$. (**F** and **G**) mRNA expression of *Fosl2* and *Arid5a* in TAMs from Catnb$^{f/f}$Lysm^{Cre}, Lysm^{Cre}, and Catnb$^{f/f}$ in (F) carcinogen-induced and (G) BMT lung tumor models, $n = 5$, **$P < 0.01$, ****$P < 0.0001$ versus Catnb$^{f/f}$. Western blot of β-catenin, FOSL2, and ARID5A in (**H**) M0, M1, M2, (**I**) M0, and M1-like and M2-like TAMs. (**J**) Scheme showing ChIP using a β-catenin antibody. (**K**) Real-time PCR of FOSL2, ARID5A, IL10, and CCND1 in β-catenin ChIP assays performed in THP1-derived M2 macrophages treated with control (DMSO) and XAV939 (5 μM) for 24 hours, $n = 6$, ****$P < 0.0001$ versus Ab_β-catenin.

(*IL1B*, *IL8*, and *CCR7*) remained unchanged in M2-like TAMs transfected with si_FOSL2 (fig. S9, D and E). The treatment of A549 cells with CM isolated from M2-like TAMs transfected with si_FOSL2 led to a decrease in their survival and proliferation (fig. S9F). This indicates that β-catenin–mediated activation of FOSL2 induces lung tumorigenicity by triggering the protumorigenic transcriptional program of M2-like macrophages. Furthermore, to ascertain the role of ARID5A repression in the polarization of M2-like TAMs, these cells were transfected with an ARID5A overexpression plasmid (OE_ARID5A; Fig. 6E and fig. S9G). Notably, the mRNA expressions of M1 macrophage markers (*TNF*, *IL8*, *CCR7*, and *IL6*) were significantly up-regulated by this intervention (Fig. 6F), whereas those of certain M1 (*IL1B*) and M2 macrophage markers (*IL10*, *CD163*, *ALOX15*, *CD206*, and *IL1R1*) remained unchanged (fig. S9, H and I). CM from M2-like TAMs transfected with OE_ARID5A led to decreased survival and proliferation of A549 cells (fig. S9J). These findings indicate that β-catenin–mediated repression of ARID5A contributes to the lung tumorigenicity by suppressing the M1-like antitumorigenic transcriptional program in M2-like macrophages.

Further, to test the specificity of XAV939 on the Catnb KO system, bone marrow–derived M0 macrophages isolated from Lysm^{Cre} and Catnb$^{f/f}$ Lysm^{Cre} mice were treated with 5 μM XAV939 for 24 hours. The Lysm^{Cre} M0 macrophage treatment with XAV939 led to a significant up-regulation of M1 macrophage-associated TF (*Arid5a*) and genes (*Tnf*, *Nos2*, and *Il1b*) and down-regulation of M2 macrophage-associated TF (*Fosl2*) and genes (*Il10*, *Arg1*, and *Chit1*). Notably, the treatment of Catnb$^{f/f}$ Lysm^{Cre} M0 macrophages with XAV939 did not result in any changes in both M1 and M2 macrophage-associated TFs or genes (fig. S9, K and L). These findings confirm the specificity of β-catenin–dependent M2 macrophage polarization via the transcriptional regulation of *Fosl2* and *Arid5a*.

High expression of β-catenin and FOSL2 and low expression of ARID5A are correlated with poor survival in patients with lung cancer

Survival analysis, using transcriptomic data of patients with lung cancer, was performed to understand the clinical significance of

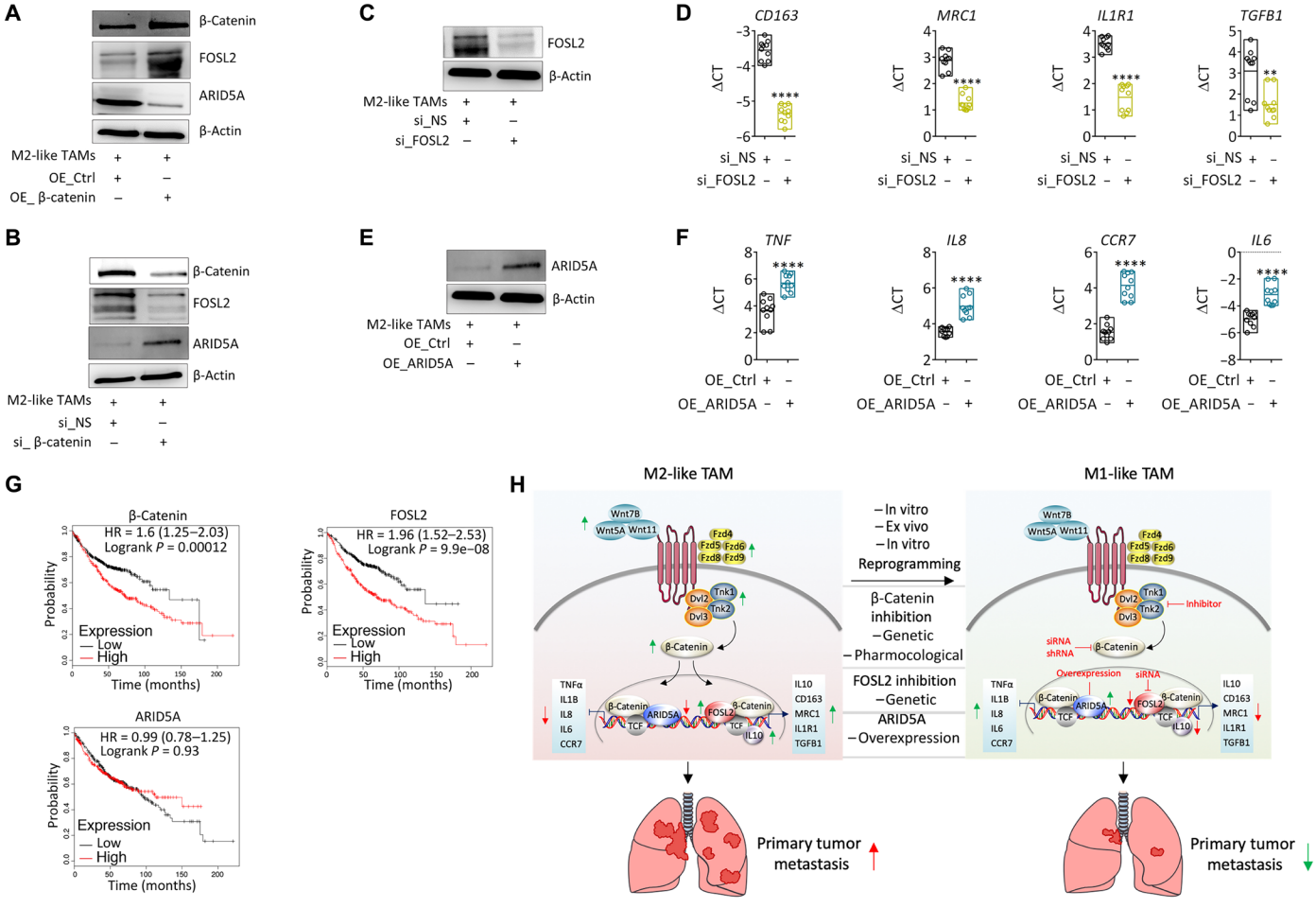

Fig. 6. Inhibition of Wnt/β-catenin signaling and FOSL2 and activation of ARID5A switch phenotype to M1-like TAMs; correlation of β-catenin/FOSL2/ARID5A with the survival of lung cancer patients. Western blot of β-catenin, FOSL2, and ARID5A in M2-like TAMs transfected with (**A**) OE_NS, OE_β-catenin, (**B**) si_NS, and si_β-catenin. (**C**) Western blot of FOSL2. (**D**) mRNA expression of *CD163*, *MRC1*, *IL1R1*, and *TGFB1* in M2-like TAMs with si_NS and si_FOSL2. (**E**) Western blot of ARID5A. (**F**) mRNA expression of *TNF*, *IL8*, *CCR7*, and *IL6* in M2-like TAMs with OE_NS and OE_ARID5A, $n = 10$, $^{**}P < 0.01$, $^{****}P < 0.0001$ versus si_NS or OE_NS. (**G**) Kaplan-Meier survival analysis of lung adenocarcinoma patients stratified by β-catenin, FOSL2, and ARID5A expression. HR, hazard ratio. (**H**) M2-like TAMs show up-regulation of WNT ligands (5A-7B-11), frizzled receptors (4-5-6-8-9), disheveled (2-3), and TNKS (1-2), leading to transcriptional activation of β-catenin. β-Catenin activates M2-macrophage program by binding to promoter region of M2 macrophage genes (IL10) and to TF-activating M2 macrophage genes, FOSL2 (CD163, MRC1, IL1R1, and TGFB1). In addition, β-catenin represses M1 macrophage program by binding to TF-activating M1 macrophage genes, ARID5A (TNFα, IL8, CCR7, and IL6). Therefore, in vitro trained, ex vivo cultured, and in vivo β-catenin-KO M2-like TAMs are reprogramed into M1-like TAMs by genetic and pharmacological inhibition of β-catenin, knockdown of FOSL2, and overexpression of ARID5A. These results indicate the reactivation of antitumor immunity in TME to restrict primary and metastatic lung tumor growth.

β-catenin, FOSL2, and ARID5A expressions in lung TME (*26*). Notably, Kaplan-Meier curves illustrated that low expression of β-catenin and FOSL2 and high expression of ARID5A in patients with lung cancer result in improved patient survival (Fig. 6G). This observation strongly supports the relevance of the previously unacknowledged role of β-catenin–mediated transcriptional regulation of FOSL2 and ARID5A in the phenotypic transition of TAMs in lung TME, thereby contributing to tumor biology. Therefore, as schematically summarized in Fig. 6H, targeting β-catenin and specific downstream TFs offers a new therapeutic concept to efficiently reprogram M2-like TAMs to M1-like TAMs, thereby repressing the transcriptional program of protumorigenic M2 macrophages, activating the antitumorigenic transcriptional program of M1 macrophages, and reducing lung tumor growth and metastasis.

DISCUSSION

In the present study, we provide strong evidence that β-catenin–mediated transcription plays a central role in the transition of tumor-inhibiting M1-like TAMs to tumor-promoting M2-like TAMs. Therefore, targeting β-catenin in TAMs may provide a new immunotherapeutic option to reactivate antitumor immunity in lung TME. This concept (summarized in Fig. 6H) is based on the following key findings. First, Wnt/β-catenin signaling (expression and nuclear β-catenin activity) is significantly activated in TAMs isolated from patients with lung cancer and in M2-like TAMs "trained" by coculturing with primary lung cancer cells or a lung cancer cell line compared with their M1 counterparts. Second, genetic or pharmacological ablation of nuclear β-catenin activity in primary TAMs isolated from human and mouse lung tumors, as well as in in vitro trained M2-like TAMs, phenotypically and functionally "reprograms" M2-like

TAMs to M1-like TAMs. Third, pharmacological and macrophage-specific genetic ablation of β-catenin in five different in vivo lung tumor models reduce primary and metastatic lung tumor growth, together with reactivation of the antitumor response of M1-like TAMs in lung TME. Last, β-catenin–mediated transcriptional activation of FOSL2 (a TF regulating the M2 macrophage–specific gene signature) and repression of ARID5A (a TF regulating the M1 macrophage–specific gene signature) play a prominent role in the phenotypic transition of TAMs. Several histopathological and experimental studies reported a prominent signature and prognostic importance of macrophages in lung TME (*5*, *6*, *27*). Classically, macrophages are divided into two subtypes: M1 macrophages (generated by LPS/IFNγ) and alternatively activated M2 macrophages (generated by IL4). Emerging evidence suggests that in the classical method of macrophage polarization, extrinsic and intrinsic characteristics of macrophages vary according to cytokines stimulation conditions (*28*), and the gene regulation in cytokine-stimulated macrophages may not be similar to TAMs (*8*, *29*). Therefore, the dualistic definition of M1/M2 macrophages based on cytokine stimulation is limited and may not be applicable to TAMs, which are present in spatial proximity to tumor cells and other tumor-infiltrating immune cells in TME; therefore, they receive a multitude of activating signals (*30*, *31*). Therefore, we performed RNA-seq of TAMs isolated from patients with lung cancer and matched controls to dissect the molecular signature of these tumor-infiltrating macrophages. In addition, we established a protocol for macrophages (by coculturing with tumor cells) to induce TAM development on a dish. This approach consistently reproduced the phenotypic and functional transition of M1-like TAMs to M2-like TAMs (when M0 macrophages cocultured with three different lung tumor cell lines and primary lung tumor cells), allowing the analysis of the underlying transcriptional changes by sequential RNA-seq. RNA-seq analysis revealed that M1-like TAMs/M2-like TAMs mimic the complexity of human TAMs, at least at the level of gene regulation as compared to classical M1/M2. In addition, this analysis disclosed that TAM-specific Wnt/β-catenin signaling plays a key role in the lung cancer cell–driven phenotypic transition of antitumorigenic M1-like TAMs to protumorigenic M2-like TAMs. In addition, we performed (i) coimmunostaining of β-catenin and CD68 in a human lung tissue microarray, (ii) protein expression analysis of Wnt/β-catenin signaling and its target genes in three different in vitro TAM models, and (iii) assessment of nuclear β-catenin activity by nuclear/cytoplasmic fractionation and TCF/LEF luciferase activity assay. These investigations clearly demonstrated that Wnt/β-catenin signaling is strongly activated in M2-like TAMs, unlike in M1-like TAMs, as well as in human TAMs in lung cancer tissues. Consistent with this notion, the data reported by Zilionis *et al.* (*29*), wherein single-cell RNA sequencing (scRNA-seq) data of tumor-data of tumor-infiltrating immune cell populations isolated from patients with lung tumor biopsies, demonstrated an up-regulation of Wnt/β-catenin signaling–related genes in macrophages compared with other immune cell populations.

The postulated central role of Wnt/β-catenin signaling in the activation of M2-like TAMs is further supported by a series of in vivo studies. In three different tumor models, the inhibition of Wnt/β-catenin signaling significantly reduced primary and metastatic lung tumor growth by reprogramming TAMs into tumor-inhibiting M1-like TAM phenotype. These results confirmed that β-catenin inhibition not only affects tumor cells but also switches the TAM phenotype in vivo. Furthermore, to precisely investigate the contribution of macrophage-specific β-catenin to experimental lung tumorigenesis, two lung tumor models were used in β-catenin knockout mice ($Catnb^{f/f}Lysm^{Cre}$): (i) carcinogen-induced lung tumor model, $Catnb^{f/f}Lysm^{Cre}$ mice showed reduced lung tumor growth compared to $Lysm^{Cre}$ and $Catnb^{f/f}$, and (ii) bone marrow transplantation model, Lysm is expressed not only by macrophages but also by neutrophil/DCs and epithelial cells. Thus, to exclude any Lysm-mediated targeting effect of epithelial cells, we transplanted bone marrow cells isolated from $Lysm^{Cre}$, $Catnb^{f/f}$, and $Catnb^{f/f}Lysm^{Cre}$ mice into lethally irradiated WT mice, followed by intratracheal injection of LLC1 cells. Notably, we observed 60 to 70% reduction of macroscopic and microscopic lung tumor burden in WT mice that received bone marrow cells isolated from $Catnb^{f/f}Lysm^{Cre}$ mice compared with in WT mice that received bone marrow cells isolated from $Lysm^{Cre}$ or $Catnb^{f/f}$ mice. In both the models, β-catenin_KO_TAMs (TAM_$Catnb^{f/f}Lysm^{Cre}$) have M1-like TAM phenotype. Although the role of DCs and neutrophils cannot be excluded, this provides an (in) direct evidence that macrophage-specific β-catenin plays a major role in lung cancer progression.

Spranger *et al.* (*32*) demonstrated that in human melanoma tumors, the activation of β-catenin prevents CCL4 gene expression, which further leads to T cell exclusion. In this study, we observed increased mRNA expression of CCL4 upon the inhibition of β-catenin in M2-like TAMs, postulating that interference in the TAM-specific Wnt/β-catenin pathway recruits other antigen-presenting cells to overcome immune evasion.

Many inhibitors targeting Wnt/β-catenin signaling are in different phases of clinical trials. However, no safe and effective inhibitor has been moved to clinical practice. The major obstacles for the clinical use of β-catenin inhibitors are not only the common issues of pharmacological activity and safety related to new drug development but also strategies used for its targeting. In previous studies, Wnt/β-catenin signaling interference was primarily considered to directly affect cancer cells (*19*, *33*, *34*). However, our study ascertains that macrophage-specific β-catenin targeting is a potential and sufficient therapeutic strategy to treat lung cancer based on the following findings. (i) The genetic and pharmacological inhibition of β-catenin phenotypically and functionally reprograms M2-like TAMs to M1-like TAMs, and inhibition in M1-like TAMs augments its antitumor effects. (ii) In vitro dose-comparison study suggests that reactivation of antitumor response in M2-like TAMs requires less amount of pharmacological inhibitor of β-catenin when compared to direct treatment to tumor cells. (iii) Further comparison of tumor cell functions and the TAM polarization status upon genetic and pharmacological ablation of β-catenin in tumor cells versus macrophages suggested that β-catenin ablation in tumor cells influences only tumor cell functions with no subsequent influence on the TAM polarization status, whereas β-catenin ablation in TAMs influences both tumor cell function and the TAM polarization status. Further evidence comparing macrophage-specific and tumor cell–specific β-catenin modulation in the same in vivo tumor model will unequivocally prove that compared to tumor cell–specific β-catenin targeting, macrophage-specific β-catenin targeting is a potent therapeutic option for the lung cancer.

Increased TNFα activity plays a key role in blocking of the M2 polarization pathway (*23*–*25*). Previously, we demonstrated that CCR2/CX3CR1 signaling plays a central role in tumor cell–macrophage cross-talk (*6*), and a recent publication by Ou *et al.* (*22*) suggested a positive feedback loop between β-catenin and CCR2. However, our

data suggest that β-catenin–modulated TNFα and CCR2/β-catenin axis only partially regulates the β-catenin–mediated transition of macrophage phenotype. Therefore, to understand the β-catenin–mediated transcriptional landscape that drives the reprogramming of TAMs, we performed extensive analysis of M2-like TAMs with the gain of function and loss of function of β-catenin. These results revealed that β-catenin–mediated regulation of TFs such as FOSL2 and ARID5A is responsible for the phenotypic and functional transition of M1-like TAMs to M2-like TAMs. β-Catenin positively regulated FOSL2 transcription, whereas it negatively regulated that of ARID5A. The gain of function of ARID5A in M2-like TAMs exclusively up-regulated the M1 macrophage gene signature (TNFα, IL1B, CCR7, and IL6), whereas loss of function of FOSL2 in M2-like TAMs exclusively down-regulated the M2 macrophage gene signature (CD163, CD206, IL1R1, and TGFB1), accompanied by functional antitumor effects on the survival and proliferation of lung tumor cells. Several other studies have demonstrated the oncogenic potential of FOSL2 in the growth and metastasis of tumor cells (*35*–*37*). However, none of these studies investigated whether the currently described M2-to-M1 phenotypic macrophage transition in TME may underlie such efficacy. Therefore, apart from β-catenin, our study also highlights potential new targets (FOSL2 and ARID5A) to unleash antitumor M1-like TAM responses in lung TME.

In corroboration of these experimental and molecular studies, the analysis of the transcriptomic dataset of a large number of patients with lung cancer showed low expressions of β-catenin and FOSL2 and high expression of ARID5A to be significantly correlated with improved patient survival. However, future studies should assess clinical outcomes based on TAM-specific β-catenin/FOSL2/ARID5A expression to assess the survival advantage provided by a TAM-specific inhibitor of β-catenin and its transcriptional targets (FOSL2 and ARID5A) in the treatment of lung cancer. In conclusion, β-catenin–mediated transcriptional activation of FOSL2 and repression of ARID5A play a pivotal role in the phenotypic and functional transition of tumor-inhibiting M1-like TAMs to tumor-promoting M2-like TAMs in lung cancer. Thus, TAM-specific inhibition of Wnt/β-catenin and its downstream signaling pathways controlling the M1-to-M2 phenotypic transition of TAM in TME may offer a new therapeutic strategy for the treatment of lung cancer while possibly minimizing the side effects associated with broad Wnt/β-catenin inhibition.

MATERIALS AND METHODS

Cancer cell lines

We purchased human tumor cell lines (A549, A427, H1650, and THP1) and mouse LLC1 cells from the American Type Culture Collection and cultured according to the manufacturer's instructions. We cultured A549 cells in Dulbecco's modified Eagle's medium supplemented with 10% fetal calf serum (FCS) and 1% penicillin/streptomycin (P/S). A427, H1650, and LLC1 cells were cultured in RPMI 1640 medium supplemented with 10% FCS and 1% P/S. Further, we cultured THP1 cells in RPMI 1640 medium supplemented with 10% FCS, 1% P/S, and 5% Hepes.

Primary cancer cell culture

The University of Giessen Biobank provided cancer cells isolated from human lung tumors (NSCLC). We grew cells in Dulbecco's modified Eagle's medium F12 (supplemented with sodium selenite, ethanolamine, phosphoryl ethanolamine, sodium pyruvate, adenine, and Hepes). We maintained them for a maximum of seven to eight passages.

Generation and activation of human and mouse macrophages

We generated murine macrophages from bone marrow and human macrophages from blood monocytes as previously described. Briefly, human macrophages were differentiated from peripheral blood mononuclear cells (PBMCs) isolated from buffy coats obtained from the blood bank of the Universities of Giessen and Marburg Lung Center using Ficoll density gradient centrifugation. We seeded the macrophages on tissue culture–treated six-well plates (Sarstedt, Nümbrecht, Germany). After culturing PBMCs for 1 hour in RPMI 1640 supplemented with 1% P/S, we removed nonadherent cells and cultured them in a macrophage medium (RPMI 1640 medium supplemented with 2% human serum and 1% P/S) for 7 days to allow differentiation from monocytes to macrophages. The density of macrophages was roughly 1×10^5 cells per well in six-well plates. Regarding mouse macrophages, we dissected the tibia and femur from mice, and each bone was subsequently flushed thrice with 5 ml of RPMI 1640 medium supplemented with 1% P/S. The cells went through a 40-μM cell strainer, centrifuged, and resuspended in RPMI 1640 medium supplemented with 10% FCS, 1% P/S, and mouse macrophage colony-stimulating factor (M-CSF; 20 ng/ml; Roche, Mannheim, Germany) and plated on a six-well plate. We changed the medium on alternate days with RPMI 1640 medium supplemented with 10% FCS, 1% P/S, and mouse M-CSF (20 ng/ml) until undifferentiated macrophages were obtained. We treated THP1 cells with phorbol 12-myristate-12 acetate (10 ng/ml) for 24 hours and then removed them for 24 hours before differentiation. Further, we activated or polarized human and mouse macrophages. We obtained M1 macrophages through M0 stimulation with LPS (100 ng/ml) and IFNγ (100 U/ml) for 24 hours, whereas to obtain M2 macrophages, we stimulated M0 macrophages with IL4 (20 ng/ml) for 24 hours (*6*, *7*).

Generation of in vitro trained TAMs

To generate TAMs, we harvested cancer cells with trypsin-EDTA, washed them once with cancer cell medium (supplemented with 10% FCS and 1% P/S), and subsequently resuspended them in macrophage medium. We cultured macrophages and cancer cells in a 1:1 ratio (1×10^5 tumor cells:1×10^5 macrophages per six-well plate in 2 ml of medium) in macrophage medium for 3 days. Subsequently, the medium in the culture dish was discarded. We detached the remaining cancer cells using 500 μl of trypsin-EDTA (3 min) and removed them from the culture dish. We washed the macrophages in the six wells thrice with 2 ml of macrophage medium and further incubated them in macrophage medium for 1 hour at 37°C. Subsequently, we added new cancer cells (1×10^5) to the culture dish containing macrophages (previously cultured with cancer cells for 3 days) in a 1:1 ratio for further 2 days. To obtain pure macrophages at the end of the coculture, we discarded the medium in the culture dish. The remaining cancer cells were detached using trypsin-EDTA and removed from the culture dish (*38*, *39*). At different time points, we collected macrophages and tumor cells for FACS, RNA (TRIzol), protein expression [radioimmunoprecipitation assay (RIPA) buffer], and cellular assays. Further, we transfected or treated attached macrophages (days 3 and 5) with the required agents, as described in the following sections (*38*, *39*).

Treatment with XAV939

We treated A549 cells (1, 2, 4, 8, 16, 32, 64, and 128 μM), M2-like TAMs (1, 2, 4, 5, and 8 μM), and ex vivo TAMs from human and mouse lung tumors with XAV939 (5 μM; Tocris, Wiesbaden-Nordenstadt, Germany) and M2-like TAMs with RS 504393 (5 μM; Tocris, Wiesbaden-Nordenstadt, Germany) as per the 3-(4,5-dimethylthiazol-2-yl)-2,5-diphenyltetrazolium bromide (MTT) assay protocol and a previous study (*40*) for 24 hours at 37°C.

Transfection with siRNA and shRNA

Concerning siRNA, we transfected macrophages with different siRNAs using the HiPerFect Transfection Reagent (Qiagen, Hilden, Germany) in an optimum serum-free medium (Sigma-Aldrich, Taufkirchen, Germany). β-Catenin siRNA, FOSL2 siRNA, and AllStars negative siRNA as nonsilencing control (si_NS) were obtained from Qiagen (Qiagen, Hilden, Germany). According to the protocol provided by the manufacturer, we transfected the cells with siRNA for 6 hours in the serum-free medium. After 6 hours, we cultured the cells in a serum-containing macrophage medium for 24 hours.

Concerning shRNA, we transfected macrophages with different shRNAs using the jetPEI-Macrophage kit (Polyplus Transfection, Illkirch-Graffenstaden, France). We obtained β-catenin shRNA, EG5 positive control shRNA, and nonsilencing shRNA (sh_NS) from GE Dharmacon (Lafayette, CO, USA). According to the protocol provided by the manufacturer, we mixed shRNA (1.5 μg) and a transfection reagent (3 μl) for one well of a six-well plate and incubated for 30 min at room temperature (RT) to allow the formation of complexes. Subsequently, we added a mixture dropwise on the macrophages in a serum-containing medium, and we incubated the mixture for 24 hours at 37°C to allow transfection of cells.

Transfection with plasmid

We transfected M2-like TAMs with different plasmids (β-catenin and ARID5A) using the Viromer RED kit (Lipocalyx, Halle, Germany). β-Catenin, ARID5A, and negative plasmid (OE_Ctrl) were obtained from GeneCopoeia (Rockville, MD, USA). Before transfection, cells were serum-starved for 24 hours. According to the protocol provided by the manufacturer, we mixed plasmid (2 μg) and transfection reagent (2.4 μl) in a six-well plate and incubated them for 30 min at RT to form complexes. Subsequently, we added a serum-containing medium dropwise to the transfection mixture, and the mixture was incubated for 24 hours at 37°C (*39*).

Proliferation assay and apoptosis assay

We seeded tumor cells (1×10^4 cells per well) on a 96-well plate for 24 hours, followed by serum starvation for 24 hours. Following serum starvation, we treated the cells with different CM for 24 hours, such as CM from M0, M1, M2 macrophages, in vitro trained M1-like TAMs, M2-like TAMs, M2-like TAMs and M2-like TAMs treated with DMSO, 5 μM XAV939, M2-like TAMs transfected with sh_EG5; sh_NS; sh_β-catenin; and M2-like TAMs transfected with si_NS, si_FOSL2, OE_Ctrl, OE_ARID5A, and OE_β-catenin. We treated primary tumor cells with CM isolated from M0 macrophages, in vitro trained M1-like TAMs, M2-like TAMs, CM from human ex vivo TAMs treated with DMSO, 5 μM XAV939, CM from human ex vivo TAMs transfected with si_NS, and si_β-catenin. We treated LLC1 cells with CM isolated from mouse ex vivo TAMs treated with DMSO and 5 μM XAV939. The following day, we assessed proliferation and apoptosis using a bromodeoxyuridine cell proliferation assay kit (Roche) and a cell death detection kit (Roche), respectively (*6*, *7*).

Migration assay

We quantified migratory tumor cells after different CM treatment using a Boyden chamber transwell assay. We added CM (700 μl per well) to a 24-well companion plate with a 0.8 μM pore size insert (BD Biosciences, San Jose, CA, USA). Further, we seeded 5×10^4 cells/300 μl medium in the upper part of each insert and incubated for 6 hours at 37°C. Subsequently, we washed transwell inserts with phosphate-buffered saline (PBS) and placed them in methanol for fixation, followed by 10-min crystal violet staining. After washing with distilled water, each membrane was mounted on slides with Pertex (Medite GmbH, Burgdorf, Switzerland). The slides were scanned with NanoZoomer 2.0-HT digital slide scanner C9600 (Hamamatsu Photonics). We quantified the number of migratory cells per membrane using ImageJ software (National Institutes of Health, Bethesda, MD, USA) as previously described (*6*, *7*, *41*).

RNA isolation, complementary DNA synthesis, and quantitative PCR

We extracted total mRNA from cell pellets using the miRNeasy Micro Kit (Qiagen). Further, we subsequently transcribed RNA into complementary DNA using the kit according to the manufacturer's instructions. Quantitative PCR was performed with SYBR Green Supermix kit (Bio-Rad, Dreieich, Germany). Intron-spanning human- and mouse-specific primer genes were designed using sequence information obtained from the National Center for Biotechnology Information database and purchased from Sigma-Aldrich. Expression was determined using the ΔCT method. We normalized the CT values to housekeeping gene–encoding hypoxanthine-guanine phosphoribosyltransferase using the equation $\Delta CT = CT_{reference} - CT_{target}$ and expressed as ΔCT. The primer sequences used in this study are shown in table S1.

Western blotting

We lysed cells in RIPA lysis buffer containing protease and phosphatase inhibitors. Subsequently, we cleared the lysate through high-speed centrifugation. Proteins were separated using 10% polyacrylamide gels and transferred to polyvinylidene difluoride membranes. After blocking with 5% milk, we incubated the membranes with a primary antibody overnight at 4°C on a rotating platform. After washing with tris-buffered saline and Tween 20, we incubated the blots with secondary antibodies conjugated to horseradish peroxidase. We detected bound protein-antibody conjugates using an enhanced chemiluminescence detection system. The Western blots shown in figures are representative of three independent experiments. The details of the antibodies are shown in table S2.

Quantification of TNF and IL10 by ELISA

The concentrations of TNF and IL10 in CM from M0, M1, M2, M1-like TAMs, and M2-like TAMs were quantified using the Human TNF-alpha Quantikine ELISA (enzyme-linked immunosorbent assay) Kit and Human IL-10 Quantikine ELISA Kit (R&D Systems) as per the manufacturer's instructions.

Nucleocytoplasmic extraction of β-catenin from in vitro trained TAMs

We conducted extraction of nuclear and cytoplasmic β-catenin from M1-like and M2-like TAMs using NE-PER Nuclear and Cytoplasmic

Extraction Reagents (Thermo Fisher Scientific) as per the manufacturer's instructions.

TCF/LEF luciferase activity assay

We cotransfected macrophages (M0, M1-like TAMs, and M2-like TAMs) in six-well plates using TCF/LEF luciferase construct (0.3 μg per well) and Renilla luciferase construct (10 ng per well; Promega) using Lipofectamine 2000 transfection reagent for 6 hours in optimum serum-free medium. After 6 hours, we incubated cells with serum-containing medium for 24 hours at 37°C. We quantified luciferase activities using the dual-luciferase reporter assay system (Promega) according to the manufacturer's instructions and a spectrofluorometer (Tecan Infinite M200 PRO plate reader). The ratio of luciferase signal–to–Renilla signal for each well was calculated as previously described (*42*).

Chromatin immunoprecipitation

We treated approximately 10×10^6 macrophages (THP1-derived M2 macrophages) with XAV939 (5 μM) for 24 hours and assessed through ChIP. We cross-linked cells by adding one-tenth volume of a cross-linking solution [11% formaldehyde, 0.1 M sodium chloride, 1 mM EDTA, 0.5 mM egtazic acid, and 50 mM Hepes (pH 8)] overnight at 4°C. The following day, the reaction was terminated by adding 0.125 M glycine. We washed cells thrice with ice-cold PBS for 5 min, and we obtained the nuclear cell fraction through sequential lysis with L1 and L2 lysis buffers. The cell lysate in L2 buffer was sonicated using the Diagenode Bioruptor (Seraing, Belgium) with 3- × 30-s pulses (30-s pause between pulses). We removed cell debris through high-speed centrifugation. The resulting chromatin extract, containing DNA fragments with an average size of 500 base pair, was immunoprecipitated overnight at 4°C using Salmon Sperm DNA/Protein A Agarose beads (Merck Millipore, Darmstadt, Germany), which had been preincubated with 5 μg of an appropriate antibody. The following day, after washing, elution, and reverse cross-linking, we purified DNA using a PCR purification kit (Qiagen) (*43*). We quantified purified DNA via SYBR Green real-time PCR (Bio-Rad) using specific primers (table S1). Data are expressed as percentage of input and calculated using this formula: % of input = $2^{(-dCT)}$ [dCT = CT ChIP – (CT Input – $\log_2$ dilution factor)].

Human lung tissues

The lung tissue microarray LUC1501 contains 150 cores from tissue samples comprising normal/benign (n = 2) and cancer (n = 70, graded according to the Tumor, Node, Metastasis staging system) cases, with duplicated cores for each case (catalog no. LUC1501, Pantomics Inc., Richmond, CA, USA). We obtained lung tissue specimens in RPMI medium supplemented with cycloheximide (10 μg/ml) obtained from the Institute for Pathology (Giessen, Germany). We stored tissue specimens at 4°C on the day of collection and processed on the following day. The study protocol for tissue donation was approved by the Ethics Committee ("Ethik Kommission am Fachbereich Humannmedizin der Justus Liebig Universität Giessen") of the University Hospital Giessen (Giessen, Germany) in accordance with the national law and "Good Clinical Practice/International Conference on Harmonisation" guidelines. Written informed consent was provided by each patient or the patient's next of kin (AZ 58/15).

Immunofluorescence staining

We deparaffinized the slide with LUC1501 by heating for 1 hour at 60°C and immersion in xylene for 30 min. We sequentially rehydrated tissues using 99, 96, and 70% ethanol and iso-propanol. We performed antigen retrieval by heating tissues in citrate buffer for 30 min, followed by washing them with 1× PBS and blocking in 5% bovine serum albumin (BSA) at RT for 1 hour. We subsequently washed the slides thrice with 1× PBS and incubated them with primary antibodies for β-catenin and CD68 overnight at 4°C. Then, we washed the slides thrice with 1× PBS and incubated them with the secondary antibodies Alexa Fluor 488 goat antirabbit immunoglobulin G (IgG) and Alexa Fluor 555 goat anti-mouse IgG for 1 hour at RT. We rewashed the slides thrice with 1× PBS and incubated with 4′,6-diamidino-2-phenylindole (1100) at RT for 15 min to stain nuclei, followed by a 5-min wash with 1× PBS and mounting with the DAKO tissue-mounting medium (Agilent, CA, USA). We visualized the slides under a confocal microscope (Zeiss LSM 710) using the Zen 2011 software (*7*, *41*). The details of the antibodies are shown in table S2.

Animal experiments

We maintained all mice under specific pathogen-free conditions and handled them in accordance with the guidelines of the European Union Commission on Laboratory Animals. C57BL/6, Catnb$^{f/f}$ (B6.129-Ctnnb1tm2Kem/KnwJ), and Lysm^{Cre} (B6.129P2-Lyz2tm1(cre) Ifo/J) mice were purchased from the Jackson laboratory (Bar Harbor, ME, USA). We generated Catnb$^{f/f}$Lysm^{Cre} mice by crossbreeding mice. All animal experiments were performed at the Max Planck Institute for Heart and Lung Research (Bad Nauheim, Germany), which were approved by local authorities (Regierungspräsidium Darmstadt, Hessen, Germany), and at the University of Patras (Patras, Greece). In this project, these lung tumor models were used. (i) For the subcutaneous tumor model, we subcutaneously injected mouse LLC1 cells (1×10^6) into C57BL/6 mice. On day 20, we euthanized the mice and harvested tumors as previously described (*6*). (ii) For the carcinogen-induced lung tumor model, we chemically induced lung adenocarcinoma in C57BL/6 and transgenic mice (Catnb$^{f/f}$Lysm^{Cre}, Catnb$^{f/f}$, and Lysm^{Cre}) by 10 consecutive weekly intraperitoneal exposures to urethane (1 g/kg) for 5 months, followed by XAV939 treatment, and we euthanized mice on day 26 following the first injection of XAV939 (*44*). (iii) For the primary lung tumor model, intratracheal instillation of 1×10^6 LLC1 cells and quantification were performed as previously described (*6*). (iv) For metastasis, we used a tumor relapse model by inducing tumors in C57BL/6 mice through subcutaneous injection of 1×10^6 LLC1 cells. On day 10, subcutaneous tumors were resected, followed by wound closure and XAV939 treatment. All mice were carefully examined and euthanized as previously described (*6*).

Treatment of mice with XAV939

We intraperitoneally treated mice with XAV939 (25 mg/kg) on every third day until the aforementioned endpoints of the respective tumor models were reached. Further, we photographed the subcutaneous tumors or lungs. Notably, we used subcutaneous tumor (0.4 gm) or the right lung to prepare single-cell suspension for FACS analysis and magnetic cell sorter (MACS) sorting of F4/80$^+$ macrophages. The remaining subcutaneous tumors or the left lung was immersed in 4% paraformaldehyde (PFA), followed by embedding in paraffin for histological examination.

Bone marrow transplantation model

We lethally irradiated C57BL/6 mice after total body irradiation (1100 rad). Twelve hours after irradiation, we reconstituted C57BL/6 mice with bone marrow transplant (BMT) from transgenic mice

($Catnb^{f/f}Lysm^{Cre}$, $Catnb^{f/f}$, and $Lysm^{Cre}$) by providing 1×10^7 bone marrow cells retro-orbitally. On day 30 after transplantation, we completed full bone marrow reconstitution (*45*) and intratracheally injected 1×10^6 LLC1 cells into mice as previously described (*6*). On day 16, we photographed the lungs. We used the right lung to prepare single-cell suspension for FACS analysis and MACS sorting of $F4/80^+$ macrophages, whereas we immersed the left lung in 4% PFA, followed by embedding in paraffin for histological examination.

MACS sorting of TAMs from human and mouse lung tumor tissues

We prepared single-cell suspensions from human lung tumors using the Tumor Dissociation Kit (Miltenyi Biotec, Bergisch Gladbach, Germany) according to the manufacturer's instructions. Macrophages from these single-cell suspensions were magnetically sorted using primary antibodies, human CD68-PE (phycoerythrin) (Miltenyi Biotec) and secondary antibody, anti-PE MicroBeads (Miltenyi Biotec) according to the instructions provided by the manufacturer. Patient characteristics are shown in table S3. We fragmented mouse tumor tissues into small pieces, followed by digestion with collagenase (5 μg/μl) supplemented with deoxyribonuclease (DNase; 10 μg/μl) for 30 min at 37°C. Further, we passed the tissue extract through a cell strainer and treated it with red blood cell lysis buffer. Subsequently, we centrifuged and suspended cells in MACS buffer (Miltenyi Biotec, Bergisch Gladbach, Germany) supplemented with 5% BSA. We magnetically sorted macrophages from single-cell suspensions using the primary antibody F4/80-PE mouse (Miltenyi Biotec, Bergisch Gladbach, Germany) and the secondary antibody anti-PE MicroBeads (Miltenyi Biotec, Bergisch Gladbach, Germany), according to the instructions provided by the manufacturers.

Flow cytometry and cell sorting

We blocked single-cell suspensions with a FcR blocking reagent (Miltenyi Biotec) in 0.5% PBS-BSA for 20 min, stained them with fluorochrome-conjugated antibodies, and analyzed them on an LSR II/Fortessa flow cytometer or sorted them using a FACS Aria III cell sorter (both from BD Biosciences). We analyzed data using FlowJo V10 (TreeStar). All antibodies and secondary reagents were titrated to determine optimal concentrations. Comp-Beads (BD Biosciences) were used for single-color compensation to create multicolor compensation matrices. For gating, we used fluorescence minus one control. We controlled instrument calibration daily using Cytometer Setup and Tracking beads (BD Biosciences). For characterization and sorting of immune cell subsets in mouse tumors, we used the following antibodies: anti–CD3-PE-CF594, anti–CD4-BV510, anti–CD8-BV650, anti–CD11b-BV605, anti–CD11c-AlexaFluor700, anti–CD19-APC-H7, anti–CD326-BV711, anti–Ly6C-Per-CP-Cy5.5 (BD Biosciences), anti–CD45-Vio-Blu, anti–MHC-II-APC (Miltenyi Biotec), anti–CD80-PE, anti–F4/80-PE-Cy7, anti–CD206-FITC, and anti–Ly6G-APC-Cy7 (BioLegend). For the characterization and sorting of human macrophages, single-cell suspensions were stained with the following antibodies: anti–CD33-BV510, anti–CD45-AlexaFluor700, anti–CD64-BV605, anti–CD83-BV711 (BD Biosciences), anti–CD163-PE, anti–CD206-PE-Cy7, and anti–CD326-FITC (BioLegend). We used 7-Aminoactinomycin D (7-AAD) to exclude dead cells. For analyzing macrophage viability in cocultures, macrophages were harvested as described in the "Generation of in vitro trained TAMs" section and stained with anti-CD64-BV605 to exclude remaining tumor cells and with AnnexinV-BV421 and 7-AAD (all from BD Biosciences) to determine the amount of living versus dead cells.

Hematoxylin and eosin staining

We deparaffinized tissue sections by heating for 1 hour at 60°C and immersion in xylene for 30 min. We sequentially rehydrated tissues by 99, 96, and 70% ethanol and isopropanol. We immersed the sections in hematoxylin (Invitrogen Corporation, Frederick, MD, USA) for 20 min, followed by washing with distilled water and immersion in acidified eosin solution (Richard-Allan Scientific, Kalamazoo, MI, USA) for 4 min. After the final wash with distilled water, we sequentially dehydrated sections through immersion in 96 and 99% ethanol and xylene, followed by mounting with the tissue-mounting medium Pertex (Medite GmbH, Burgdorf, Switzerland).

Lung tumor quantification

At the end of the animal experiment, we euthanized the mice. We collected and processed their lungs for histopathology as previously described. Briefly, we dissected and embedded tissue blocks from all left lung lobes in paraffin. We generated serial sections (50 to 80 μm) from each lung tissue block. We stained these sections with hematoxylin and eosin and analyzed them under a light microscope (Leica Instruments) for the presence of tumor cell clusters. We performed the analysis in a blinded fashion.

Bioinformatics analysis

For RNA-seq, we isolated RNA from primary macrophages (NMs and TAMs from human lung tissue; $n = 5$), in vitro trained TAMs (A549 in vitro trained M1-like TAMs and M2-like TAMs; $n = 3$), and β-catenin–knockdown M2-like TAMs (M2-like TAMs transfected with control_shRNA and β-catenin_shRNA; $n = 3$) using the miRNeasy micro Kit (Qiagen) combined with on-column DNase digestion (DNase-Free DNase Set, Qiagen) to avoid contamination by genomic DNA. We verified RNA and library preparation integrity with Bioanalyzer 2100 (Agilent) or LabChip GX Touch 24 (PerkinElmer). For in vitro trained TAMs and β-catenin–knockdown M2-like TAMs, we used total RNA (3 μg) as an input for the preparation of the TruSeq Stranded mRNA Library following the low sample protocol (Illumina). We used total RNA (1 μg) from primary macrophages as input for SMARTer Stranded Total RNA Sample Prep Kit-HI Mammalian (Clontech). We performed sequencing on the NextSeq500 instrument (Illumina) using v2 chemistry with 1- × 75-bp single-end setup.

We assessed the resulting raw reads for quality, adapter content, and duplication rates with FastQC (available online at: www.bioinformatics.babraham.ac.uk/projects/fastqc). Trimmomatic version 0.36 was used to trim reads after a reduction in quality below a mean of Q15 in a window of five nucleotides. Only reads longer than 15 nt were cleared for further analysis. We aligned trimmed and filtered reads versus the Ensembl human genome version hg38 (GRCh38.27) using STAR 2.5.4b with the parameter "--outFilterMismatchNoverLmax 0.1" to increase the maximum ratio of mismatches to mapped length of up to 10%. The number of reads aligning to genes was counted using the featureCounts 1.6.0 tool from the Subread package. Only reads mapping at least partially inside exons were admitted and aggregated per gene. We excluded reads overlapping multiple genes or aligning to multiple regions. We identified differentially expressed genes (DEGs) using DESeq2 version 1.14.1 (*46*). The Ensembl annotation was enriched with Universal

Protein Resource data based on Ensembl gene identifiers. For the RNA-seq of primary macrophages, genes were classified as significantly differentially expressed at an average count of >5 ($P < 0.05$ and $-0.29 \leq \log_2FC \geq +0.29$). For the RNA-seq of in vitro trained TAMs, the raw count matrix was normalized using DESeq2 version 1.18.1 (*46*). Because strong biological biases could not be effectively normalized using batch correction algorithms, we independently computed $\log_2$ transformed fold changes for each biological replicate and contrast. We assumed genes to be differentially expressed when all three biological replicates showed a $\log_2$ fold change of ≥ 0.585 or ≤ -0.585, and the mean normalized expression was ≥ 30. For the RNA-seq of β-catenin–knockdown M2-like TAMs, Reaper version 13-100 was used to trim reads after a reduction in quality below a mean of Q20 in a window of 20 nucleotides. We classified genes as significantly differentially expressed at an average count of >5 using the Benjamini-Hochberg procedure (corrected $P < 0.05$).

We performed a secondary analysis of all samples combined including batch correction to show the correlation of all datasets when applying similar algorithmic treatment (seen in Venn diagram in Fig. 1K). The samples were initially processed as described previously. A combined raw count matrix was produced and batch corrected per dataset using CountClust (*47*). The batch-corrected matrix was taken for differential expression analysis with DESeq2 version 1.26.0 (*46*). Genes were classified as significantly differentially expressed at an average count of >5, multiple testing adjusted $P < 0.1$, and $-0.29 \leq \log_2FC \geq +0.29$.

Analysis of pathway enrichment using KOBAS

DEGs were tested for gene set overrepresentation using KOBAS (*48*). Two separate tests were performed per contrast using only either up- or down-regulated genes for analysis. The results were combined, keeping only gene sets that showed significant overrepresentation at false discovery rate (FDR) < 0.2 in only one input list (i.e., that were either clearly enriched for up- or down-regulated genes, but not both). The top 10 gene sets considering enrichment FDR were selected per direction of regulation.

Statistical analysis

We analyzed all data using Prism 5.0 and Prism 6.0 (GraphPad Software). We performed statistical comparisons between two groups using Student's *t* test. For comparisons among >2 groups, we performed one-way analysis of variance followed by Tukey's posttest. All data are expressed as means ± SE of the mean. A *P* value of ≤0.05 denoted statistical significance.

SUPPLEMENTARY MATERIALS

Supplementary material for this article is available at http://advances.sciencemag.org/cgi/content/full/6/23/eaaz6105/DC1

View/request a protocol for this paper from *Bio-protocol*.

REFERENCES AND NOTES

1. R. L. Siegel, K. D. Miller, A. Jemal, Cancer statistics, 2019. *CA Cancer J. Clin.* **69**, 7–34 (2019).
2. S. L. Topalian, F. S. Hodi, J. R. Brahmer, S. N. Gettinger, D. C. Smith, D. F. McDermott, J. D. Powderly, R. D. Carvajal, J. A. Sosman, M. B. Atkins, P. D. Leming, D. R. Spigel, S. J. Antonia, L. Horn, C. G. Drake, D. M. Pardoll, L. Chen, W. H. Sharfman, R. A. Anders, J. M. Taube, T. L. McMiller, H. Xu, A. J. Korman, M. Jure-Kunkel, S. Agrawal, D. McDonald, G. D. Kollia, A. Gupta, J. M. Wigginton, M. Sznol, Safety, activity, and immune correlates of anti-PD-1 antibody in cancer. *N. Engl. J. Med.* **366**, 2443–2454 (2012).
3. C. Y. Ock, J. E. Hwang, B. Keam, S. B. Kim, J. J. Shim, H. J. Jang, S. Park, B. H. Sohn, M. Cha, J. A. Ajani, S. Kopetz, K. W. Lee, T. M. Kim, D. S. Heo, J. S. Lee, Genomic landscape associated with potential response to anti-CTLA-4 treatment in cancers. *Nat. Commun.* **8**, 1050 (2017).
4. V. Thorsson, D. L. Gibbs, S. D. Brown, D. Wolf, D. S. Bortone, T. H. Ou Yang, E. Porta-Pardo, G. F. Gao, C. L. Plaisier, J. A. Eddy, E. Ziv, A. C. Culhane, E. O. Paull, I. K. A. Sivakumar, A. J. Gentles, R. Malhotra, F. Farshidfar, A. Colaprico, J. S. Parker, L. E. Mose, N. S. Vo, J. Liu, Y. Liu, J. Rader, V. Dhankani, S. M. Reynolds, R. Bowlby, A. Califano, A. D. Cherniack, D. Anastassiou, D. Bedognetti, Y. Mokrab, A. M. Newman, A. Rao, K. Chen, A. Krasnitz, H. Hu, T. M. Malta, H. Noushmehr, C. S. Pedamallu, S. Bullman, A. I. Ojesina, A. Lamb, W. Zhou, H. Shen, T. K. Choueiri, J. N. Weinstein, J. Guinney, J. Saltz, R. A. Holt, C. S. Rabkin; Cancer Genome Atlas Research Network, A. J. Lazar, J. S. Serody, E. G. Demicco, M. L. Disis, B. G. Vincent, I. Shmulevich, The immune landscape of cancer. *Immunity* **48**, 812–830.e14 (2018).
5. M. Rakaee, L. T. R. Busund, S. Jamaly, E. E. Paulsen, E. Richardsen, S. Andersen, S. Al-Saad, R. M. Bremnes, T. Donnem, T. K. Kilvaer, Prognostic value of macrophage phenotypes in resectable non-small cell lung cancer assessed by multiplex immunohistochemistry. *Neoplasia* **21**, 282–293 (2019).
6. A. Schmall, H. M. al-tamari, S. Herold, M. Kampschulte, A. Weigert, A. Wietelmann, N. Vipotnik, F. Grimminger, W. Seeger, S. S. Pullamsetti, R. Savai, Macrophage and cancer cell cross-talk via CCR2 and CX3CR1 is a fundamental mechanism driving lung cancer. *Am. J. Respir. Crit. Care Med.* **191**, 437–447 (2015).
7. S. S. Pullamsetti, B. Kojonazarov, S. Storn, H. Gall, Y. Salazar, J. Wolf, A. Weigert, N. el-Nikhely, H. A. Ghofrani, G. A. Krombach, L. Fink, S. Gattenlöhner, U. R. Rapp, R. T. Schermuly, F. Grimminger, W. Seeger, R. Savai, Lung cancer-associated pulmonary hypertension: Role of microenvironmental inflammation based on tumor cell-immune cell cross-talk. *Sci. Transl. Med.* **9**, eaai9048 (2017).
8. R. D. Stout, C. Jiang, B. Matta, I. Tietzel, S. K. Watkins, J. Suttles, Macrophages sequentially change their functional phenotype in response to changes in microenvironmental influences. *J. Immunol.* **175**, 342–349 (2005).
9. X. Zheng, K. Turkowski, J. Mora, B. Brüne, W. Seeger, A. Weigert, R. Savai, Redirecting tumor-associated macrophages to become tumoricidal effectors as a novel strategy for cancer therapy. *Oncotarget* **8**, 48436–48452 (2017).
10. G. Akiri, M. M. Cherian, S. Vijayakumar, G. Liu, A. Bafico, S. A. Aaronson, Wnt pathway aberrations including autocrine Wnt activation occur at high frequency in human non-small-cell lung carcinoma. *Oncogene* **28**, 2163–2172 (2009).
11. L. Kren, M. Hermanová, V. N. Goncharuk, P. Kaur, J. S. Ross, Z. Pavlovský, K. Dvorák, Downregulation of plasma membrane expression/cytoplasmic accumulation of β-catenin predicts shortened survival in non-small cell lung cancer. A clinicopathologic study of 100 cases. *Cesk. Patol.* **39**, 17–20 (2003).
12. J. Jin, P. Zhan, M. Katoh, S. S. Kobayashi, K. Phan, H. Qian, H. Li, X. Wang, X. Wang, Y. Song; written on behalf of the AME Lung Cancer Collaborative Group, Prognostic significance of β-catenin expression in patients with non-small cell lung cancer: A meta-analysis. *Transl. Lung Cancer Res.* **6**, 97–108 (2017).
13. D. J. Stewart, Wnt signaling pathway in non-small cell lung cancer. *J. Natl. Cancer Inst.* **106**, djt356 (2014).
14. D. J. Stewart, Tumor and host factors that may limit efficacy of chemotherapy in non-small cell and small cell lung cancer. *Crit. Rev. Oncol. Hematol.* **75**, 173–234 (2010).
15. M. Liu, X. Sun, S. Shi, MORC2 enhances tumor growth by promoting angiogenesis and tumor-associated macrophage recruitment via Wnt/β-catenin in lung cancer. *Cell. Physiol. Biochem.* **51**, 1679–1694 (2018).
16. J. J. Luke, R. Bao, R. F. Sweis, S. Spranger, T. F. Gajewski, WNT/β-catenin pathway activation correlates with immune exclusion across human cancers. *Clin. Cancer Res.* **25**, 3074–3083 (2019).
17. S. G. Pai, B. A. Carneiro, J. M. Mota, R. Costa, C. A. Leite, R. Barroso-Sousa, J. B. Kaplan, Y. K. Chae, F. J. Giles, Wnt/β-catenin pathway: Modulating anticancer immune response. *J. Hematol. Oncol.* **10**, 101 (2017).
18. E. J. Yeo, L. Cassetta, B. Z. Qian, I. Lewkowich, J. F. Li, J. A. Stefater III, A. N. Smith, L. S. Wiechmann, Y. Wang, J. W. Pollard, R. A. Lang, Myeloid WNT7b mediates the angiogenic switch and metastasis in breast cancer. *Cancer Res.* **74**, 2962–2973 (2014).
19. T. Valenta, G. Hausmann, K. Basler, The many faces and functions of β-catenin. *EMBO J.* **31**, 2714–2736 (2012).
20. A. Weigert, N. Tzieply, A. von Knethen, A. M. Johann, H. Schmidt, G. Geisslinger, B. Brüne, Tumor cell apoptosis polarizes macrophages–Role of sphingosine-1-phosphate. *Mol. Biol. Cell* **18**, 3810–3819 (2007).
21. S. Edin, M. L. Wikberg, J. Rutegård, P. A. Oldenborg, R. Palmqvist, Phenotypic skewing of macrophages in vitro by secreted factors from colorectal cancer cells. *PLOS One* **8**, e74982 (2013).
22. B. Ou, X. Cheng, Z. Xu, C. Chen, X. Shen, J. Zhao, A. Lu, A positive feedback loop of β-catenin/CCR2 axis promotes regorafenib resistance in colorectal cancer. *Cell Death Dis.* **10**, 643 (2019).
23. F. Kratochvill, G. Neale, J. M. Haverkamp, L. A. van de Velde, A. M. Smith, D. Kawauchi, J. McEvoy, M. F. Roussel, M. A. Dyer, J. E. Qualls, P. J. Murray, TNF counterbalances the emergence of M2 tumor macrophages. *Cell Rep.* **12**, 1902–1914 (2015).

24. U. Schleicher, K. Paduch, A. Debus, S. Obermeyer, T. König, J. C. Kling, E. Ribechini, D. Dudziak, D. Mougiakakos, P. J. Murray, R. Ostuni, H. Körner, C. Bogdan, TNF-mediated restriction of arginase 1 expression in myeloid cells triggers type 2 NO synthase activity at the site of infection. *cell rep.* **15**, 1062–1075 (2016).
25. P. J. Murray, Macrophage polarization. *Annu. Rev. Physiol.* **79**, 541–566 (2017).
26. B. Győrffy, P. Surowiak, J. Budczies, A. Lánczky, Online survival analysis software to assess the prognostic value of biomarkers using transcriptomic data in non-small-cell lung cancer. *PLOS One* **8**, e82241 (2013).
27. G. A. Banat, A. Tretyn, S. S. Pullamsetti, J. Wilhelm, A. Weigert, C. Olesch, K. Ebel, T. Stiewe, F. Grimminger, W. Seeger, L. Fink, R. Savai, Immune and inflammatory cell composition of human lung cancer stroma. *PLOS One* **10**, e0139073 (2015).
28. P. J. Murray, J. E. Allen, S. K. Biswas, E. A. Fisher, D. W. Gilroy, S. Goerdt, S. Gordon, J. A. Hamilton, L. B. Ivashkiv, T. Lawrence, M. Locati, A. Mantovani, F. O. Martinez, J. L. Mege, D. M. Mosser, G. Natoli, J. P. Saeij, J. L. Schultze, K. A. Shirey, A. Sica, J. Suttles, I. Udalova, J. A. van Ginderachter, S. N. Vogel, T. A. Wynn, Macrophage activation and polarization: Nomenclature and experimental guidelines. *Immunity* **41**, 14–20 (2014).
29. R. Zilionis, C. Engblom, C. Pfirschke, V. Savova, D. Zemmour, H. D. Saatcioglu, I. Krishnan, G. Maroni, C. V. Meyerovitz, C. M. Kerwin, S. Choi, W. G. Richards, A. de Rienzo, D. G. Tenen, R. Bueno, E. Levantini, M. J. Pittet, A. M. Klein, Single-cell transcriptomics of human and mouse lung cancers reveals conserved myeloid populations across individuals and species. *Immunity* **50**, 1317–1334.e10 (2019).
30. M. Chittezhath, M. K. Dhillon, J. Y. Lim, D. Laoui, I. N. Shalova, Y. L. Teo, J. Chen, R. Kamaraj, L. Raman, J. Lum, T. P. Thamboo, E. Chiong, F. Zolezzi, H. Yang, J. A. van Ginderachter, M. Poidinger, A. S. C. Wong, S. K. Biswas, Molecular profiling reveals a tumor-promoting phenotype of monocytes and macrophages in human cancer progression. *Immunity* **41**, 815–829 (2014).
31. L. Cassetta, S. Fragkogianni, A. H. Sims, A. Swierczak, L. M. Forrester, H. Zhang, D. Y. H. Soong, T. Cotechini, P. Anur, E. Y. Lin, A. Fidanza, M. Lopez-Yrigoyen, M. R. Millar, A. Urman, Z. Ai, P. T. Spellman, E. S. Hwang, J. M. Dixon, L. Wiechmann, L. M. Coussens, H. O. Smith, J. W. Pollard, Human tumor-associated macrophage and monocyte transcriptional landscapes reveal cancer-specific reprogramming, biomarkers, and therapeutic targets. *Cancer Cell* **35**, 588–602.e10 (2019).
32. S. Spranger, R. Bao, T. F. Gajewski, Melanoma-intrinsic β-catenin signalling prevents anti-tumour immunity. *Nature* **523**, 231–235 (2015).
33. D. Dangaj, D. Barras, G. Coukos, Tumor landscapes: β-catenin drives immune desertification. *Clin. Cancer Res.* **25**, 2943–2945 (2019).
34. M. Kahn, Can we safely target the WNT pathway? *Nat. Rev. Drug Discov.* **13**, 513–532 (2014).
35. L. Gao, Y. N. Guo, J. H. Zeng, F. C. Ma, J. Luo, H. W. Zhu, S. Xia, K. L. Wei, G. Chen, The expression, significance and function of cancer susceptibility candidate 9 in lung squamous cell carcinoma: A bioinformatics and in vitro investigation. *Int. J. Oncol.* **54**, 1651–1664 (2019).
36. J. Wang, D. Sun, Y. Wang, F. Ren, S. Pang, D. Wang, S. Xu, FOSL2 positively regulates TGF-β1 signalling in non-small cell lung cancer. *PLOS One* **9**, e112150 (2014).
37. T. Nakayama, K. Hieshima, T. Arao, Z. Jin, D. Nagakubo, A. K. Shirakawa, Y. Yamada, M. Fujii, N. Oiso, A. Kawada, K. Nishio, O. Yoshie, Aberrant expression of Fra-2 promotes CCR4 expression and cell proliferation in adult T-cell leukemia. *Oncogene* **27**, 3221–3232 (2008).
38. B. Weichand, R. Popp, S. Dziumbla, J. Mora, E. Strack, E. Elwakeel, A. C. Frank, K. Scholich, S. Pierre, S. N. Syed, C. Olesch, J. Ringleb, B. Ören, C. Döring, R. Savai, M. Jung, A. von Knethen, B. Levkau, I. Fleming, A. Weigert, B. Brüne, S1PR1 on tumor-associated macrophages promotes lymphangiogenesis and metastasis via NLRP3/IL-1β. *J. Exp. Med.* **214**, 2695–2713 (2017).
39. J. Ringleb, E. Strack, C. Angioni, G. Geisslinger, D. Steinhilber, A. Weigert, B. Brüne, Apoptotic cancer cells suppress 5-lipoxygenase in tumor-associated macrophages. *J. Immunol.* **200**, 857–868 (2018).
40. C. Li, X. Zheng, Y. Han, Y. Lv, F. Lan, J. Zhao, XAV939 inhibits the proliferation and migration of lung adenocarcinoma A549 cells through the WNT pathway. *Oncol. Lett.* **15**, 8973–8982 (2018).
41. R. Savai, H. M. Al-Tamari, D. Sedding, B. Kojonazarov, C. Muecke, R. Teske, M. R. Capecchi, N. Weissmann, F. Grimminger, W. Seeger, R. T. Schermuly, S. S. Pullamsetti, Pro-proliferative and inflammatory signaling converge on FoxO1 transcription factor in pulmonary hypertension. *Nat. Med.* **20**, 1289–1300 (2014).
42. S. S. Pullamsetti, G. A. Banat, A. Schmall, M. Szibor, D. Pomagruk, J. Hänze, E. Kolosionek, J. Wilhelm, T. Braun, F. Grimminger, W. Seeger, R. T. Schermuly, R. Savai, Phosphodiesterase-4 promotes proliferation and angiogenesis of lung cancer by crosstalk with HIF. *Oncogene* **32**, 1121–1134 (2013).
43. F. Yi, L. Pereira, J. A. Hoffman, B. R. Shy, C. M. Yuen, D. R. Liu, B. J. Merrill, Opposing effects of Tcf3 and Tcf1 control Wnt stimulation of embryonic stem cell self-renewal. *Nat. Cell Biol.* **13**, 762–770 (2011).
44. G. T. Stathopoulos, T. P. Sherrill, D. S. Cheng, R. M. Scoggins, W. Han, V. V. Polosukhin, L. Connelly, F. E. Yull, B. Fingleton, T. S. Blackwell, Epithelial NF-κB activation promotes urethane-induced lung carcinogenesis. *Proc. Natl. Acad. Sci. U.S.A.* **104**, 18514–18519 (2007).
45. T. Agalioti, A. D. Giannou, A. C. Krontira, N. I. Kanellakis, D. Kati, M. Vreka, M. Pepe, M. Spella, I. Lilis, D. E. Zazara, E. Nikolouli, N. Spiropoulou, A. Papadakis, K. Papadia, A. Voulgaridis, V. Harokopos, P. Stamou, S. Meiners, O. Eickelberg, L. A. Snyder, S. G. Antimisiaris, D. Kardamakis, I. Psallidas, A. Marazioti, G. T. Stathopoulos, Mutant *KRAS* promotes malignant pleural effusion formation. *Nat. Commun.* **8**, 15205 (2017).
46. M. I. Love, W. Huber, S. Anders, Moderated estimation of fold change and dispersion for RNA-seq data with DESeq2. *Genome Biol.* **15**, 550 (2014).
47. K. K. Dey, C. J. Hsiao, M. Stephens, Visualizing the structure of RNA-seq expression data using grade of membership models. *PLOS Genet.* **13**, e1006599 (2017).
48. C. Xie, X. Mao, J. Huang, Y. Ding, J. Wu, S. Dong, L. Kong, G. Gao, C. Y. Li, L. Wei, KOBAS 2.0: A web server for annotation and identification of enriched pathways and diseases. *Nucleic Acids Res.* **39**, W316–W322 (2011).

Acknowledgments: We thank Y. Knepper, V. Golchert, and P. Mathoor for excellent technical assistance. We thank G. Lilis and G. Ntaliarda for helping in BMT experiments, P. Chelladuari for the support in ChIP establishment, and K. Turkoswki for help with the animal experiment proposal. **Funding:** This work was supported by the Max Planck Society, Verein zur Förderung der Krebsforschung in Gießen e.V., Von-Behring-Röntgen-Stiftung, a Rhön Klinikum AG grant, Frankfurt Cancer Institute (LOEWE FCI), Cardio-Pulmonary Institute (CPI), the German Center for Lung Research (DZL) and DFG, SFB 1213 (Project A01, A05 to S.S.P.). G.A.G. and G.T.S. were supported by the European Research Council Starting Independent Investigator (#260524 to G.T.S.), Proof of Concept Grants (#679345 to G.T.S.), and Consolidator Grant (#866051 to S.S.P.).
Competing interests: The authors declare that they have no competing interests. **Author contributions:** R.S., S.S.P., and W.S. designed the experiments and supervised the study. P.S., X.Z., G.A.G., A.W., and A.F. carried out the cell culture, molecular, FACS, immunohistochemical, and animal experiments. R.S. and G.T.S. designed and supervised animal experiments. C.K. and S.G. performed RNA-seq and bioinformatics. S. Ga. and F.G. provided human lung tumor samples. T.S. and B.B. generated and provided essential reagents. P.S., R.S., S.S.P., and W.S. wrote the manuscript. All authors reviewed and edited the paper. **Data and materials availability:** All data needed to evaluate the conclusions in the paper are present in the paper and/or the Supplementary Materials. Additional data related to this paper may be requested from the authors.

Submitted 24 September 2019
Accepted 27 March 2020
Published 5 June 2020
10.1126/sciadv.aaz6105

Citation: P. Sarode, X. Zheng, G. A. Giotopoulou, A. Weigert, C. Kuenne, S. Günther, A. Friedrich, S. Gattenlöhner, T. Stiewe, B. Brüne, F. Grimminger, G. T. Stathopoulos, S. S. Pullamsetti, W. Seeger, R. Savai, Reprogramming of tumor-associated macrophages by targeting β-catenin/FOSL2/ARID5A signaling: A potential treatment of lung cancer. *Sci. Adv.* **6**, eaaz6105 (2020).

ScienceAdvances

Reprogramming of tumor-associated macrophages by targeting β-catenin/FOSL2/ARID5A signaling: A potential treatment of lung cancer

Poonam Sarode, Xiang Zheng, Georgia A. Giotopoulou, Andreas Weigert, Carste Kuenne, Stefan Günther, Aleksandra Friedrich, Stefan Gattenlöhner, Thorsten Stiewe, Bernhard Brüne, Friedrich Grimminger, Georgios T. Stathopoulos, Soni Savai Pullamsetti, Werner Seeger and Rajkumar Savai

Sci Adv **6** (23), eaaz6105.
DOI: 10.1126/sciadv.aaz6105

Science Advances (ISSN 2375-2548) is published by the American Association for the Advancement of Science, 1200 New York Avenue NW, Washington, DC 20005. The title *Science Advances* is a registered trademark of AAAS.